International Journal of Computational Fluid Dynamics, Vol. 19, No. 5, July 2005, 359–380

Taylor & Francis
Taylor & Francis Group

Local time-stepping procedures for the space-time conservation element and solution element method

SIN-CHUNG CHANG†, YUHUI WU‡, VIGOR YANG‡* and XIAO-YEN WANG†

†NASA Glenn Research Center, Cleveland, Ohio 44135, USA
‡Pennsylvania State University, University Park, PA 16802, USA

(Received 24 October 2003; in final form 25 January 2005)

A local time-stepping procedure for the space-time conservation element and solution element (CESE) method has been developed. This new procedure allows for variation of time-step size in both space and time, and can also be extended to become multi-dimensional solvers with structured/unstructured spatial grids. Moreover, it differs substantially in concept and methodology from the existing approaches. By taking full advantage of key concepts of the CESE method, in a simple and efficient manner it can enforce flux conservation across an interface separating grid zones of different time-step sizes. In particular, no correction pass is needed. Numerical experiments show that, for a variety of flow problems involving moving shock and flame discontinuities, accurate and robust numerical simulations can be achieved even with a reduction in time-step size on the order of 10 or higher for grids across a single interface.

Keywords: Space-time CESE method; Local time-stepping procedure; Flux conservation; Grid interface

Nomenclature

a	convection velocity
A_f	pre-exponential factor
CE	conservation element
E_2	two-dimensional Euclidean space
$\vec{h}$	space-time flux
$I(\overline{PQ}; V)$	integrated flux leaving volume V through face $\overline{PQ}$ and evaluated using $\vec{q}(P)$
$I(\overline{PQ}; G; V)$	integrated flux leaving volume V through face $\overline{PQ}$ and evaluated using $\vec{q}(G)$
M	number of grid points in a grid zone
MW	molecular weight
$\vec{n}$	unit outward normal of a surface element on $S(V)$
p	pressure
$\vec{q}$	column matrix formed by u and u_x
q	total heat release
r	sub-grid index
R	grid refinement ratio
SE	solution element
$S(V)$	boundary of an arbitrary space-time region V
t	time
T	temperature
T_f	activation temperature
u	marching variable
u_x	spatial derivative of marching variable
u_t	time derivative of marching variable
x	space coordinate
Y_R	mass fraction of reactant

Subscripts

CJ	Chapman-Jouguet state in a self-sustained detonation
h	head end of detonation tube
j	spatial index
s	von Neumann spike in a detonation

Superscripts

$*$	numerical analogue of variables without superscript "$*$"
$\hat{}$	normalized variable
a	the a scheme
c	variable with central difference nature
w	weighted averaged variable
n	time-step index

Greek symbols

α	exponential factor in weighting function
ρ	density
Ω_1	set of the grid points (j, n) with $(j + n)$ being odd integers
Ω_2	set of the grid points (j, n) with $(j + n)$ being even integers
$\dot{\omega}_R$	mass production rate of reactant per unit volume

*Corresponding author. Tel.: +1-814-863-1502. Fax: +1-814-865-3389. E-mail: vigor@psu.edu

International Journal of Computational Fluid Dynamics
ISSN 1061-8562 print/ISSN 1029-0257 online © 2005 Taylor & Francis
http://www.tandf.co.uk/journals
DOI: 10.1080/10618560500092610

1. Introduction

In a numerical treatment of a large spatial flow domain in which steep gradients are embedded, accurate resolution of these regions may exclude the use of a uniform coarse spatial grid. On the other hand, applying a very fine uniform spatial grid over the entire domain often is not practical because of the daunting computational cost required. Thus, the use of nonuniform spatial grids in which local grid size varies with local solution gradient may become necessary. For a solver whose stability demands that the maximum local time-step size allowed decreases with the local spatial grid size, this implies that the maximum advantage on accuracy and cost can be realized by using a nonuniform spatial grid along with a local time stepping (LTS) solver. In addition to minimizing computer cost, LTS can reduce the Courant-Friedrichs-Lewy (CFL) number disparity which often gives rise to excessive local numerical dissipation. In the present work, we will develop, in the setting of the space-time conservation element and solution element (CESE) method (Chang 1995, Chang *et al.* 1998, 1999, Wang and Chang 1999a,b, Chang *et al.* 2000, Zhang *et al.* 2002, Wu *et al.* 2003, 2004), a simple and robust LTS procedure that in principle can be applied along with any given nonuniform spatial grid.

Unlike the current work, LTS is an integral part of many adaptive space-time grid refinement methods which are generally applicable only to structured rectangular grids (Berger and Oliger 1984, Berger 1987, Berger and colella 1989, Bell *et al.* 1994, Berger and LeVeque 1998). As an example, in the work of Berger and Oliger (1984), refinement is performed in both space and time so that a constant ratio of the time-step size to the spatial grid size is maintained over different grid zones. Obviously, for a finite-difference solver in which the spatial and temporal truncation errors are of the same order, this procedure is more effective in enhancing accuracy than conventional methods solely based on spatial grid refinement procedures. Moreover, for a solver whose stability depends on the CFL number and, therefore, on the ratio of the time-step size to the spatial grid size, the use of the above space-time grid refinement procedure tends not to have a negative impact on the stability requirement of the original scheme.

For a LTS procedure to be effective, the numerical solution it generates should not be seriously contaminated by spurious reflections originating from any interface separating two space-time grid zones with different local time-step sizes. As such, space-time flux conservation must be enforced at each grid interface (Berger 1987). This requirement can be easily fulfilled in the CESE setting. The CESE method is a high-resolution and genuinely multi-dimensional method for solving general conservation laws (Chang *et al.* 1998, 1999, Wang and Chang 1999a,b, Zhang *et al.* 2002). The salient features of the CESE method include: (i) a unified treatment of flow evolution in space and time; (ii) enforcement of local and global space-time flux conservation in a coherent and efficient manner; and (iii) efficient evaluation of the fluxes at the interface of any pair of conservation elements (CEs) by means of staggered space-time grids without using Riemann solvers or other flux models. As will be shown, by taking advantage of those features, the current LTS procedure differs substantially in both concept and methodology from that established by Berger and Colella (1989), Bell *et al.* (1994), and Berger and LeVeque (1998). The treatment of the grid-to-grid communication is greatly simplified, and in particular, no correction pass is needed. Furthermore, for a wide variety of flow problems involving steep gradients, a reduction in time-step size on the order of 10 or higher can be successfully carried out across a single grid interface.

The rest of the paper is organized as follows: The fundamentals of the CESE method are provided in section 2. The 1D version of the basic LTS procedure is described and justified in section 3. It is then explained how to extend this procedure to become multi-dimensional solvers with stuctured/unstructured grids. To complement the basic LTS procedure so that it is applicable even if accuracy consideration requires that the time-step-size distribution be time dependent, a set of spatial grid value reconstruction procedures is introduced in section 4. The 2D and 3D extensions of these procedures are also described. Numerical results and conclusions are presented in sections 5 and 6, respectively.

2. Fundamentals

To facilitate the development of the LTS technique within the framework of the CESE method, the fundamentals of this method are briefly reviewed in this section. Several important concepts underlying the construction of the LTS procedure are then introduced.

2.1 The a scheme

As an example, consider the scalar wave equation

$$\frac{\partial u}{\partial t} + a\frac{\partial u}{\partial x} = 0 \tag{2.1}$$

where a is a constant >0. Let $x_1 = x$ and $x_2 = t$ be the coordinates of a 2D Euclidean space E_2. Then, using Gauss' divergence theorem in the space-time E_2, one concludes that equation (2.1) is the differential form of the integral conservation law

$$\oint_{S(V)} \vec{h}\cdot d\vec{s} = 0 \tag{2.2}$$

Here $S(V)$ is the boundary of an arbitrary *space-time* region V in E_2, $\vec{h} = (au, u)$, and $d\vec{s} = d\sigma\vec{n}$, with $d\sigma$ and $\vec{n}$, respectively, being the area and the unit outward normal vector of a surface element on $S(V)$. Note that: (i) because $\vec{h}\cdot d\vec{s}$ is the *space-time* flux of $\vec{h}$ leaving the region V through the surface element $d\vec{s}$, equation (2.2) simply

states that the *space-time* flux of $\vec{h}$ is conserved over V, i.e. the total *space-time* flux of $\vec{h}$ leaving V through $S(V)$ vanishes; (ii) in E_2, $d\sigma$ is the length of a line segment on the simple closed curve $S(V)$; and (iii) all mathematical operations can be carried out as though E_2 were an ordinary two-dimensional Euclidean space.

Let Ω_1 denote the set of all space-time staggered grid points (j,n) (dots in figure 1(a)) with $(j+n)$ being odd integers. Each $(j,n) \in \Omega_1$ is associated with a solution element (SE), i.e. (j,n). By definition, SE(j,n) is the *interior* of the region bounded by a dashed curve depicted in figure 1(b). It includes a horizontal line segment, a vertical line segment, and their immediate neighborhood. Let E_2 be divided into nonoverlapping rectangular regions (see figure 1(a)) referred to as CEs. As depicted in figure 1(c) and (d), two such regions, i.e. CE$_-(j,n)$ and CE$_+(j,n)$, are associated with each interior grid point $(j,n) \in \Omega_1$. These CEs are referred to as *basic conservation elements* (BCEs). In contrast, CE(j,n) (see figure 1(e)), which is the union of CE$_-(j,n)$ and CE$_+(j,n)$, is referred to as a *compounded conservation element* (CCE). Note that, among the line segments forming the boundary of CE$_-(j,n)$, $\overline{AB}$ and $\overline{AD}$ belong to SE(j,n), while $\overline{CB}$ and $\overline{CD}$ belong to SE$(j-1,n-1)$. Similarly, the boundary of CE$_+(j,n)$ belongs to either SE(j,n) or SE$(j+1,n-1)$. Hereafter, the line segment joining points A and B will be denoted by $\overline{AB}$ if it belongs to the SE centered at point A. The same line segment, however, will be denoted by $\overline{BA}$ if it belongs to the SE centered at point B.

At this juncture, a reader who is familar with the CESE method is warned that, in the current paper, the indices j and n are only allowed to be whole integers instead of both half and whole integers allowed in the past CESE practice. Moreover, the spatial grid size and time-step size denoted here by Δx and Δt, respectively, were represented by $\Delta x/2$ and $\Delta t/2$ in the past practice, respectively. As will be seen, these and other changes in conventions and notations are introduced to avoid unnecessary complications in the current development.

For any $(j,n) \in \Omega_1$ and any $(x,t) \in$ SE(j,n), $u(x,t)$ and $\vec{h}(x,t)$, respectively, are approximated by

$$u^*(x,t;j,n) \equiv u_j^n + (u_x)_j^n (x - x_j) + (u_t)_j^n (t - t^n) \quad (2.3)$$

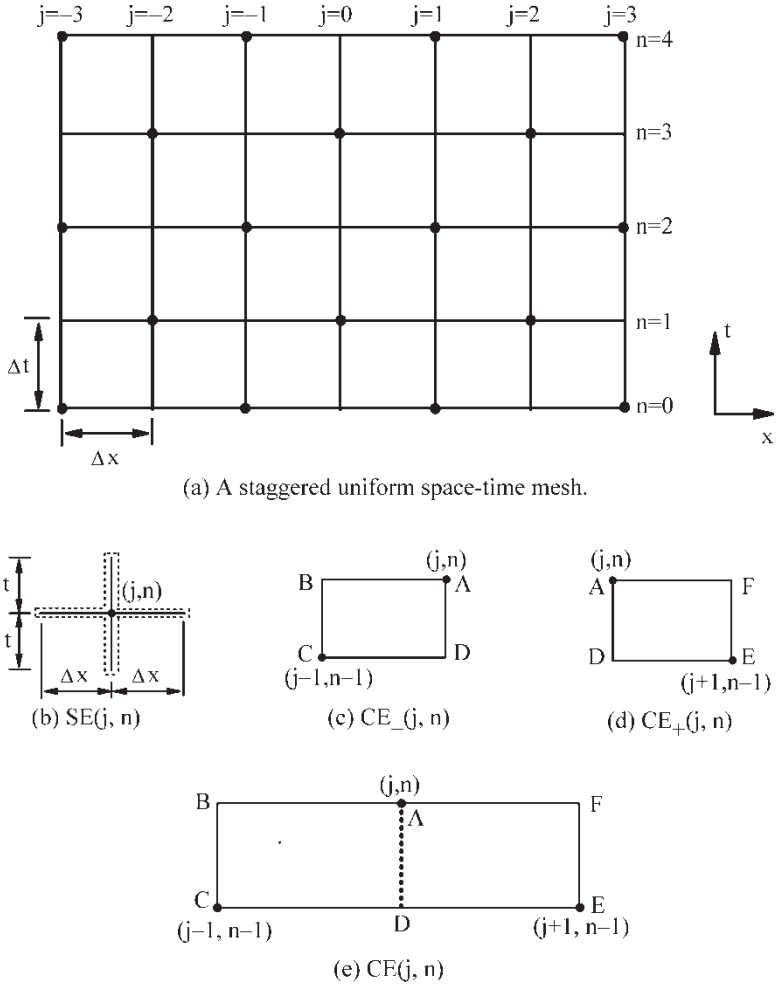

Figure 1. The solution elements (SEs) and conservation elements (CEs).

and

$$\vec{h}^*(x,t;j,n) \equiv (au^*(x,t;j,n),\ \ u^*(x,t;j,n)) \tag{2.4}$$

Here (i) u_j^n, $(u_x)_j^n$, and $(u_t)_j^n$ are constants in SE(j,n), and (ii) (x_j, t^n) are the coordinates of the grid point (j,n). The CESE method requires that $u = u^*(x,t;j,n)$ satisfy equation (2.1) within SE(j,n). As such, one has

$$(u_t)_j^n = -a(u_x)_j^n \tag{2.5}$$

Substituting equation (2.5) into equation (2.3), one has

$$u^*(x,t;j,n) = u_j^n + (u_x)_j^n[(x - x_j) - a(t - t^n)],$$
$$(x,t) \in \text{SE}(j,n) \tag{2.6}$$

Thus, u_j^n and $(u_x)_j^n$ are the only independent unknowns associated with (j,n). By imposing the following two conservation conditions

$$\oint_{S(\text{CE}_+(j,n))} \vec{h}^* \cdot d\vec{s} = 0, \ \text{and}$$
$$\oint_{S(\text{CE}_-(j,n))} \vec{h}^* \cdot d\vec{s} = 0, \quad (j,n) \in \Omega_1 \tag{2.7}$$

at each $(j,n) \in \Omega_1$, and using equations (2.4) and (2.6), one has (i)

$$u_j^n = \frac{1}{2}\Big\{(1+\nu)u_{j-1}^{n-1} + (1-\nu)u_{j+1}^{n-1} + (1-\nu^2)\Big[(\hat{u}_x)_{j-1}^{n-1} - (\hat{u}_x)_{j+1}^{n-1}\Big]\Big\} \tag{2.8}$$

and, assuming $1 - \nu^2 \neq 0$, (ii)

$$(\hat{u}_x)_j^n = (\hat{u}_x^a)_j^n \tag{2.9}$$

Here, $\nu \equiv a\Delta t/\Delta x$ and for any $(j,n) \in \Omega_1$,

$$(\hat{u}_x)_j^n \equiv \frac{\Delta x}{2}(u_x)_j^n \tag{2.10}$$

and (iii)

$$(\hat{u}_x^a)_j^n \equiv \frac{1}{2}\Big[u_{j+1}^{n-1} - u_{j-1}^{n-1} - (1-\nu) \times (\hat{u}_x)_{j-1}^{n-1} - (1+\nu)(\hat{u}_x)_{j+1}^{n-1}\Big] \tag{2.11}$$

Note that:

(a) Derivation of equations (2.8) and (2.9) can be faciliated by the following observations: Because $u^*(x,t;j,n)$ is linear in x and t, it can be shown that the total flux of $\vec{h}^*$ leaving CE$_-(j,n)$ or CE$_+(j,n)$ through any of the four line segments that form its boundary is equal to the scalar product of the vector $\vec{h}^*$ evaluated at the midpoint of the line segment and the "surface" vector (i.e. the unit outward normal multiplied by the length) of the line segment.

(b) The caret symbol in the terms $(\hat{u}_x)_j^n$ and $(\hat{u}_x^a)_j^n$ is used to denote a *normalized* paramerter. Also the symbol "a" in the term $(\hat{u}_x^a)_j^n$ is introduced to remind readers that equation (2.9) is valid for the a scheme (Chang 1995, Chang *et al.* 2000), i.e. the fundamental CESE marching scheme formed by equations (2.8) and (2.9).

Equations (2.8) and (2.9) are derived from equation (2.7). The total flux $\vec{h}^*$ leaving each of CE$_-(j,n)$ and CE$_+(j,n)$ vanishes for the a scheme. In addition, because the surface integration over any interface separating two neighboring BCEs is evaluated using the information from a single SE, the flux leaving one of these BCEs through the interface is the negative of that leaving another BCE through the same interface. As a result, the local conservation relations equation (2.7) imply that the total flux of $\vec{h}^*$ leaving the boundary of any space-time region that is the union of any combination of BCEs will also vanish, i.e. the flux of $\vec{h}^*$ is conserved over such a union. In particular, because CE(j,n) is the union of CE$_-(j,n)$ and CE$_+(j,n)$, the conservation condition

$$\oint_{S(\text{CE}(j,n))} \vec{h}^* \cdot d\vec{s} = 0, \quad (j,n) \in \Omega_1 \tag{2.12}$$

must follow from equation (2.7). In fact, it can be shown that equation (2.12) is equivalent to equation (2.8).

The a scheme is non-dissipative in its stability domain $|\nu| < 1$ and is reversible in time, i.e. the same conservation conditions equation (2.7) can be used to construct both forward and backward time marching schemes (Chang 1995). Because it cannot be extended directly to model physical problems that are irreversible in time such as an inviscid flow involving shocks, a family of dissipative solvers of equation (2.1) were constructed as extensions of the a scheme (Chang 1995). For these extensions, only the less stringent conservation condition equation (2.12) is assumed. Because equation (2.12) is equivalent to equation (2.8), each of these dissipative extensions is formed by equation (2.8) and a modified version of equation (2.9). One of such extensions will be described immediately.

2.2 *The a-α scheme*

Let $(j,n) \in \Omega_1$. With the aid of equations (2.5) and (2.10) and the definition $\nu = a\Delta t/\Delta x$, one has

$$u'^n_{j\pm1} \equiv u_{j\pm1}^{n-1} + \Delta t(u_t)_{j\pm1}^{n-1} = u_{j\pm1}^{n-1} - 2\nu(\hat{u}_x)_{j\pm1}^{n-1} \tag{2.13}$$

Because $u'^n_{j\pm1}$ is a first-order Taylor's approximation of u at $(j \pm 1,\ \ n)$,

$$(\hat{u}_x^c)_j^n \equiv \frac{u'^n_{j+1} - u'^n_{j-1}}{4} = \frac{\Delta x}{2}\left(\frac{u'^n_{j+1} - u'^n_{j-1}}{2\Delta x}\right) \tag{2.14}$$

by definition, is a central-difference approximation of $\partial u/\partial x$ at $(j,\ n,)$, normalized by the same factor $\Delta x/2$ that

appears in equation (2.10). The symbol "c" in $(\hat{u}_x^c)_j^n$ is used to denote the central-difference nature of the term $(\hat{u}_x^c)_j^n$.

Next we have

$$(\hat{u}_{x+})_j^n \equiv \frac{1}{2}(u'^n_{j+1} - u_j^n) = \frac{\Delta x}{2}\left(\frac{u'^n_{j+1} - u_j^n}{\Delta x}\right) \tag{2.15}$$

and

$$(\hat{u}_{x-})_j^n \equiv \frac{1}{2}(u_j^n - u'^n_{j-1}) = \frac{\Delta x}{2}\left(\frac{u_j^n - u'^n_{j-1}}{\Delta x}\right) \tag{2.16}$$

i.e. $(\hat{u}_{x+})_j^n$ and $(\hat{u}_{x-})_j^n$ are two normalized numerical analogues of $\partial u/\partial x$ at (j, n) with one being evaluated from the right and another from the left. Moreover, by using equations (2.14)–(2.16), one concludes that

$$(\hat{u}_x^c)_j^n = \frac{1}{2}\left[(\hat{u}_{x+})_j^n + (\hat{u}_{x-})_j^n\right] \tag{2.17}$$

i.e. $(\hat{u}_x^c)_j^n$ is the simple average of $(\hat{u}_{x+})_j^n$ and $(\hat{u}_{x-})_j^n$. Let the function W_o be defined by (i) $W_o(0, 0, \alpha) = 0$, and (ii)

$$W_o(x_-, x_+; \alpha) = \frac{|x_+|^\alpha x_- + |x_-|^\alpha x_+}{|x_+|^\alpha + |x_-|^\alpha},$$
$$(|x_+| + |x_-| > 0) \tag{2.18}$$

where x_+, x_-, and $\alpha \geq 0$ are real variables (Note: to avoid dividing by zero, in practice a small positive number such as 10^{-60} is added to the denominator in equation (2.18)). Then the a-α scheme (Chang 1995) is formed by equation (2.8) and

$$(\hat{u}_x)_j^n = (\hat{u}_x^w)_j^n \equiv W_o((\hat{u}_{x+})_j^n, (\hat{u}_{x-})_j^n;\ \ \alpha) \tag{2.19}$$

Here the superscript "w" in the term $(\hat{u}_x^w)_j^n$ is used to denote its weighted-average nature. Generally the a-α scheme is stable if $|\nu| < 1$ and $\alpha \geq 0$. Such a weighted-average nature suppresses numerical wiggles near a discontinuity if $\alpha \geq 1$ (Chang *et al.* 2000). It becomes more dissipative as α increases and the Courant number $|\nu|$ decreases. The a-α scheme has been extended to become one-dimensional and multi-dimensional Euler solvers (Chang 1995, Chang *et al.* 1999, Wang and Chang 1999a,b, Zhang *et al.* 2002). Also there are newly developed Courant-number insenstive extensions of the a-α scheme (Chang 2002, Chang and Wang 2003).

This subsection is concluded with the following remarks:

(a) Because $W_o(x_-, x_+; \alpha)$ becomes the simple average of x_- and x_+ if $\alpha = 0$ or $|x_-| = |x_+|$, one has

$$(\hat{u}_x^w)_j^n = (\hat{u}_x^c)_j^n \quad \text{if}$$
$$\alpha = 0 \ \text{ or } \ \left|(\hat{u}_{x+})_j^n\right| = \left|(\hat{u}_{x-})_j^n\right| \tag{2.20}$$

As such, the a-α scheme reduces to the scheme formed by equation (2.8) and $(\hat{u}_x)_j^n = (\hat{u}_x^c)_j^n$ in a smooth solution region (where $(\hat{u}_{x+})_j^n \approx (\hat{u}_{x-})_j^n$), even if $\alpha \neq 0$. The latter scheme is a special case of the $a - \epsilon$ scheme (Chang 1995) with $\epsilon = 1/2$. It is devoid of the special numerical dissipation associated with weight-averaging.

(b) For the a-α scheme or any other dissipative CESE solver of equation (2.1), the flux of $\vec{h}^*$ is conserved only over each CCE (see equation (2.12)), but not each BCE. Compared with the a scheme, the a-α scheme has a weaker form of global flux conservation relation, i.e. the flux of $\vec{h}^*$ *is conserved over any space-time region that is the union of any combination of CCEs*.

(c) Space-time grids that contain regions of different time-step sizes will be introduced in sections 3 and 4. For these grids, one can still define BCEs such that any space-time region can be covered by the union of a combination of *non-overlapping* BCEs. On the other hand, a space-time region may not be covered by the union of a combination of *well-defined* and *non-overlapping* CCEs. As a result, the CCE-based conservation relations of the a-α scheme established above must be reformulated as BCE-based conservation relations before they become compatible with the future development. As the first step of the reformulation, in section 2.3 the concept of *generalized flux* will be introduced and used to show that, even for the a-α scheme, the generalized flux is conserved over each BCE and over any space-time region that is the union of any combination of BCEs.

2.3 Integrated, assigned and generalized fluxes

For the a-α scheme, the flux of $\vec{h}^*$ is conserved over each CCE such as CE(j, n) shown in figure 1(e). In other words, equation (2.12) is valid if, with the aid of equations (2.4), (2.6) and (2.10),

§1 $\vec{h}^*$ at any point on $\overline{CB}$ and $\overline{CD}$ is evaluated using u_{j-1}^{n-1} and $(\hat{u}_x)_{j-1}^{n-1}$,
§2 $\vec{h}^*$ at any point on $\overline{ED}$ and $\overline{EF}$ is evaluated using u_{j+1}^{n-1} and $(\hat{u}_x)_{j+1}^{n-1}$, and
§3 $\vec{h}^*$ at any point on $\overline{AB}$ and $\overline{AF}$ is evaluated using u_j^n and $(\hat{u}_x)_j^n$.

However, for the a-α scheme, the flux of $\vec{h}^*$ is not conserved over each BCE such as CE$_-(j, n)$ and CE$_+(j, n)$ (see figure 1(c) and (d)). In other words, equation (2.7) is not valid if

§4 $\vec{h}^*$ at any point on $\overline{AD}$ (which is a part of SE(j, n)) is evaluated using u_j^n and $(\hat{u}_x)_j^n$.

Assume Rules §1–§3. Then the above discussion implies that, for the a-α scheme, the total flux leaving the boundary of CE$_-(j, n)$ vanishes only if we ignore Rule §4 and instead assume the rule:

§5 the flux leaving $CE_-(j,n)$ through $\overline{AD}$ is *assigned* to be the negative of the sum of the fluxes leaving $CE_-(j,n)$ through its other boundaries (the latter fluxes are evaluated using Rules §1 and §3).

On the other hand (also for the *a-α* scheme), the total flux leaving the boundary of $CE_+(j,n)$ vanishes only if we ignore Rule §4 and instead assume the rule:

§6 the flux leaving $CE_+(j,n)$ through $\overline{AD}$ is *assigned* to be the negative of the sum of the fluxes leaving $CE_+(j,n)$ through its other boundaries (the latter fluxes are evaluated using Rules §2 and §3).

To proceed, Rules §1–§6 are further elaborated in the following remarks:

(a) Obviously, a flux determined using any of Rules §1–§4 is fundamentally different from that determined using Rule §5 or Rule §6. The former is determined through a surface *integration* while the latter through a simple *assignment*. As such, hereafter, the former is referred to as an *integrated flux (I-flux)* while the latter an *assigned flux (A-flux)*.

(b) Note that: (i) the sum of the *I-fluxes* leaving CE(j, n) through its boundary is zero if they are evaluated using Rules §1–§3; (ii) the boundary of CE(j, n) can be divided into the line segments $\overline{AB}$, $\overline{CB}$, $\overline{CD}$, $\overline{AF}$, $\overline{EF}$, and $\overline{ED}$; (iii) the boundary of $CE_-(j,n)$ is formed by $\overline{AD}$ and the first three line segments referred to in item (ii); and (iv) the boundary of $CE_+(j,n)$ is formed by $\overline{AD}$ and the last three line segments referred to in item (ii). Thus one concludes that the A-flux leaving $CE_-(j,n)$ through $\overline{AD}$ and that leaving $CE_+(j,n)$ through $\overline{AD}$, as determined by Rules §5 and §6, respectively, are the negative of each other. In other words, *these two fluxes represent the two values of the same A-flux measured in two opposite directions.*

(c) Hereafter (see figure 1(c) and (d)), $\overline{AB}$, $\overline{CD}$, $\overline{CB}$, and $\overline{AD}$ are referred to as the top face, the bottom face, the *exterior* side face and the *interior* side face of $CE_-(j,n)$, respectively. Also, $\overline{AF}$, $\overline{ED}$, $\overline{EF}$, and $\overline{AD}$ are referred to as the top face, the bottom face, the exterior side face, and the interior side face of $CE_+(j,n)$, respectively. Note that the exterior side faces $\overline{CB}$ and $\overline{EF}$ are the side faces of CE(j, n) while the interior side face $\overline{AD}$ lies in its interior. According to the above definitions, an I-flux is defined at each of all four faces of a BCE while an A-flux is defined only at the interior side face of the BCE.

(d) For the *a* scheme, the I-flux is conserved over any BCE, i.e. the sum of the *I-fluxes* leaving any BCE through its four faces is zero. As such, Rules §5 and §6 imply that, for the *a* scheme, the I-flux and the A-flux are identical at its interior side face. However, the last assertion obviously is false for the *a-α* scheme.

Given the above preliminaries, the *generalized flux (G-flux)* leaving a BCE through its *interior* side face is defined to be the A-flux leaving the BCE through the same face, while the G-flux leaving the BCE through any one of its other three faces is defined to be the I-flux leaving the BCE through the same face. With these definitions, one concludes that, *for the a scheme, the a-α scheme and, in fact, any CESE solver that satisfies equation (2.12), the total G-flux leaving the boundary of a BCE vanishes*. Moreover, because the G-flux leaving one of any two neighboring BCEs through their interface is the negative of that leaving another BCE through the same interface, the local G-flux conservation relation eastablished above leads to a global conservation relation, i.e. *the G-flux is conserved over any space-time region that is the union of any combination of BCEs*.

G-flux is only one of two basic conceptual underpinnings of the current LTS procedure. Another is the concept of *dual flux*, a subject to be discussed in section 2.4.

2.4 Dual scheme and dual flux

In the above scheme construction, it is assumed that $(j,n) \in \Omega_1$ where Ω_1 is the set of the grid points (j, n) with $(j + n)$ being *odd* integers. The same construction can be repeated assuming $(j,n) \in \Omega_2$ where Ω_2 is the set of grid points (j,n) with $(j + n)$ being *even* integers. The grid points in Ω_2 are the unmarked points of intersection of the vertical and horizontal grid lines depicted in figure 1(a). Obviously the two CESE schemes that are constructed over Ω_1 and Ω_2, respectively, are independent of each other unless they are coupled by some relations (e.g. boundary conditions) unrelated to the internal scheme structure described above. In the following, the combination of such two schemes will be referred to as a *dual* scheme. As an example, the dual *a-α* scheme is formed by equations (2.8) and (2.19) with $(j,n) \in \Omega$ where $\Omega \equiv \Omega_1 \cup \Omega_2$.

As will be shown, *the use of dual schemes is necessary in the current LTS procedure. Its use plays a critical role in simplifying the treatment of the communications across a fine time step-coarse time step interface (i.e. an interface separating two grid zones with different local time-step sizes)*. As a preliminary, using rectangle ABCD depicted in figure 1(c) as an example, several conceptual intricacies unique to dual schemes are discussed in the following remarks:

(a) Because the grid point $(j-1,n)$ is point B depicted in figure 1(c), obviously rectangle *ABCD* is occupied by both $CE_-(j,n)$ and $CE_+(j-1,n)$. Thus a BCE is associated with two grid points, one $\in \Omega_1$ while another $\in \Omega_2$. Hereafter, these two grid points are referred to as the *cohosts* of the BCE. Moreover, to avoid confusion, from now on a space-time region such as *ABCD* will still be referred to as a BCE while a space-time region with a designated cohost such as $CE_-(j,n)$ will be

referred to as a BCE*. As such, two BCE*s can occupy the same BCE.

(b) Generally two different local I-flux conservation relations can be defined over a BCE. As an example, for the dual a scheme, the local I-flux conservation conditions

$$\oint_{S(\mathrm{CE}_-(j,n))} \vec{h}^*\cdot d\vec{s} = 0, \quad (j,n) \in \Omega_1 \tag{2.21}$$

and

$$\oint_{S(\mathrm{CE}_+(j-1,n))} \vec{h}^*\cdot d\vec{s} = 0, \quad (j-1,n) \in \Omega_2 \tag{2.22}$$

are imposed over the same BCE, i.e. rectangle *ABCD*. However, in equation (2.21), the *I-fluxes* over the four sides of *ABCD* (hereafter they are referred to as the *I-fluxes* associated with $\mathrm{CE}_-(j,n)$) are evaluated assuming (i) $\overline{AB}$ and $\overline{AD}$ belong to $\mathrm{SE}(j,n)$, and (ii) $\overline{CB}$ and $\overline{CD}$ belong to $\mathrm{SE}(j-1,n-1)$. On the other hand, in equation (2.22), the *I-fluxes* over the four sides of *ABCD* (hereafter they are referred to as the *I-fluxes* associated with $\mathrm{CE}_+(j-1,n)$) are evaluated assuming (i) $\overline{BA}$ and $\overline{BC}$ belong to $\mathrm{SE}(j-1,n)$, and (ii) $\overline{DA}$ and $\overline{DC}$ belong to $\mathrm{SE}(j,n-1)$. As a result, one concludes that: (i) two different *I-fluxes* are defined at each side of *ABCD*—one is associated with $\mathrm{CE}_-(j,n)$ while another associated with $\mathrm{CE}_+(j-1,n)$; and (ii) equations (2.21) and (2.22) represent two totally different conservation relations. According to the previously established convention, the line segment denoted by $\overline{AD}$ is considered as part of the SE centered at point A while the same line segment denoted by $\overline{DA}$ is considered as part of the SE centered at point D.

(c) Note that a side face of a BCE could be designated as an interior or exterior side face, depending on how the side face and BCE are designated. As an example, because $\overline{AD}$ lies in the interior of $\mathrm{CE}(j,n)$, by definition, $\overline{AD}$ is an interior side face of $\mathrm{CE}_-(j,n)$. On the other hand, because $\overline{DA}$ (which represents the same line segment denoted by $\overline{AD}$) lies on the exterior of $\mathrm{CE}(j-1,n)$, by definition, $\overline{DA}$ is an exterior side face of $\mathrm{CE}_+(j-1,n)$ (which shares the same space-time region *ABCD* with $\mathrm{CE}_-(j,n)$). Similarly, $\overline{CB}$ is the exterior side face of $\mathrm{CE}_-(j,n)$ while $\overline{BC}$ is the interior side face of $\mathrm{CE}_+(j-1,n)$. Thus, (i) the A-flux leaving $\mathrm{CE}_-(j,n)$ through its interior side face $\overline{AD}$, by definition, is the negative of the sum of the *I-fluxes* leaving $\mathrm{CE}_-(j,n)$ through $\overline{AB}$, $\overline{CB}$ and $\overline{CD}$; and (ii) the A-flux leaving $\mathrm{CE}_+(j-1,n)$ through its interior side face $\overline{BC}$, by definition, is the negative of the sum of the *I-fluxes* leaving $\mathrm{CE}_+(j-1,n)$ through $\overline{BA}$, $\overline{DC}$, and $\overline{DA}$.

According to the above discussions, two *I-fluxes*, one associated with $\mathrm{CE}_-(j,n)$ and another with $\mathrm{CE}_+(j-1,n)$, are defined at each face of rectangle *ABCD*. In addition, an A-flux is defined at $\overline{AD}$ (the interior side face of $\mathrm{CE}_-(j,n)$) and also at $\overline{BC}$ (the interior side face of $\mathrm{CE}_+(j-1,n)$). Let the G-flux at each face of $\mathrm{CE}_-(j,n)$ or $\mathrm{CE}_+(j-1,n)$ be defined according to the rule given previously, then there exist two different G-fluxes defined at each side of *ABCD*. In addition, the G-flux associated with $\mathrm{CE}_-(j,n)$ (or $\mathrm{CE}_+(j,n)$) is conserved over *ABCD*.

To pave the way, a BCE* associated with any $(j,n) \in \Omega_\ell (\ell = 1,2)$ will be referred to as a BCE* of Ω_ℓ. Also any G-flux associated with such a BCE* will be referred to as a G-flux of Ω_ℓ. Moreover, the *dual flux (D-flux)* at any face of a BCE is defined to be the simple average of the G-fluxes of Ω_1 and Ω_2.

For an infinite uniform grid such as that depicted in figure 1(a), Ω_1 and Ω_2 are disjoint and a CESE scheme can be applied separatively over them. Thus the two independent local G-flux conservation relations defined over a BCE lead to two independent global conservation relations, i.e. for each $\ell = 1,2$, the G-flux of Ω_ℓ is conserved over any space-time region that is the union of any combination of BCE*s of Ω_ℓ. On the other hand, for a LTS procedure defined over more complicated grids (see section 3), the grid points can not, in general, be divided into two disjoint sets over which a CESE scheme can be applied separately. Thus, for the current LTS development, the use of a dual scheme is a must and no longer there exist two independent global G-flux conservation relations. However, as will be shown, many concepts introduced above will survive and play a critical role in the LTS development. In particular, local and global D-flux conservation will be enforced in the current LTS procedure.

3. Local time stepping

In this section, the grid structure is described, and the LTS procedure and its justification are then discussed.

3.1 Grid structure

Consider the space-time grid depicted in figures 2 and 3, in which a fine-grid zone B is sandwiched between two coarse-grid zones A and C. The three grid zones are defined by

$$M_1\Delta x \geq x \geq 0 \quad (\text{zone } A) \tag{3.1}$$

$$M_2\Delta x \geq x \geq M_1\Delta x \quad (\text{zone } B) \tag{3.2}$$

and

$$M_3\Delta x \geq x \geq M_2\Delta x \quad (\text{zone } C) \tag{3.3}$$

respectively. Here (i) M_1, M_2, and M_3 are given integers with $M_1 \geq 2$, $M_2 \geq M_1 + 1$, and $M_3 \geq M_2 + 2$; and (ii) Δx and Δt, respectively, are the spatial grid size and the time-step size used in zones A and C. Their counterparts

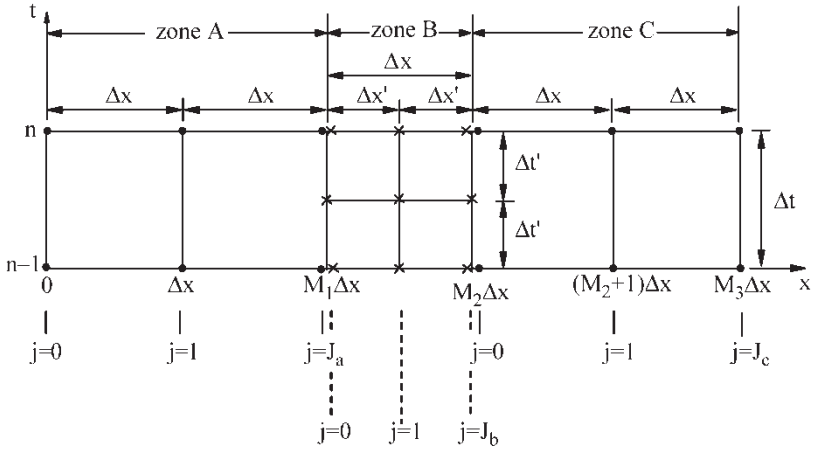

Figure 2. A computational domain containing fine and coarse grid zones ($M_1 = 2$, $M_2 = 3$, $M_3 = 5$, and $R = 2$).

used in zone B are given, respectively, by

$$\Delta x' \equiv \Delta x/R_x \quad \text{and} \quad \Delta t' \equiv \Delta t/R_t \tag{3.4a}$$

To simplify the description of the LTS procedure, and also to maintain a constant ratio of the time-step size to the spatial grid size over different grid zones, the refinement ratios R_x and R_t are assumed to satisfy the condition

$$R_x = R_t = R \tag{3.4b}$$

with $R \geq 2$ being an integer. It is worth noting that *through some straightforward modifications, the current procedure is applicable even if R_x and R_t are arbitrary positive numbers.*

In zone A, a grid point (denoted by A_j^n and marked by a dot in figure 3) is identified by a pair of indices j and n, where

$$(j,n) \in \Omega(A) \equiv \{(j,n) | j = 0, 1, 2, \ldots, J_a; \; n = 0, \pm 1, \pm 2, \ldots\} \tag{3.5}$$

with $J_a \equiv M_1$. By definition, point A_j^n is located at

$$x = x\left(A_j^n\right) \equiv j\Delta x \quad \text{and} \quad t = t\left(A_j^n\right) \equiv n\Delta t \tag{3.6}$$

In zone B, a grid point (denoted by $B_j^{n,r}$ and marked by a cross in figure 3) is identified by a triple of indices j, n and r, where

$$(j,n,r) \in \Omega(B) \equiv \{(j,n,r) | j = 0, 1, 2, \ldots, J_b; \; n = 0, \pm 1, \pm 2, \ldots; r = 0, 1, 2, \ldots, R\} \tag{3.7}$$

with $J_b \equiv (M_2 - M_1)R$. By definition, point $B_j^{n,r}$ is located at

$$x = x\left(B_j^{n,r}\right) \equiv \left(M_1 + \frac{j}{R}\right)\Delta x \quad \text{and} \quad t = t\left(B_j^{n,r}\right) \equiv \left(n + \frac{r}{R}\right)\Delta t \tag{3.8}$$

Thus, for each j, the grid points $B_j^{n-1,R}$ and $B_j^{n,0}$ share the same space-time location. They are considered as the same grid point.

In zone C, a grid point (denoted by C_j^n and marked by a dot in figure 3) is identified by a pair of indices j and n, where

$$(j,n) \in \Omega(C) \equiv \{(j,n) | j = 0, 1, 2, \ldots, J_c; \; n = 0, \pm 1, \pm 2, \ldots\} \tag{3.9}$$

with $J_c \equiv M_3 - M_2$. By definition, point C_j^n is located at

$$x = x\left(C_j^n\right) \equiv (M_2 + j)\Delta x \quad \text{and} \quad t = t\left(C_j^n\right) \equiv n\Delta t \tag{3.10}$$

Note that, for each n, points $A_{J_a}^n$ and $B_0^{n,0}$ have the same space-time location. In the LTS procedure to be described in section 3.2, two grid points with the same space-time location but belonging to different grid zones will be assigned with two *different* sets of grid variables. Consequently, such two grid points must be treated as two *different* grid points and denoted with different symbols. For clarity, in figure 2, points $A_{J_a}^n$ and $B_0^{n,0}$ ($n = 0, 1, 2, \ldots$) are moved slightly to the left and right of their exact locations, respectively. This practice also

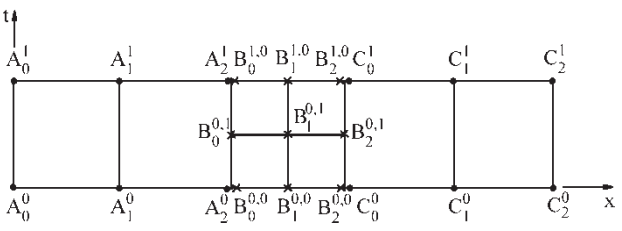

Figure 3. The grid points lying on and between the 0th and 1st time levels ($J_a = J_b = J_c = R = 2$).

applies to the grid points at the interface between zones B and C.

This concludes the discussion of grid geometry. The following are preliminary remarks on the application of several previously introduced concepts over the current more complicated grid.

(a) By definition, (i) rectangles $A_j^{n-1}A_{j+1}^{n-1}A_{j+1}^{n}A_j^{n}$, $(j,n) \in \Omega(A)$ and $j < J_a$, are the BCEs in zone A; (ii) rectangles $B_j^{n-1,r}B_{j+1}^{n-1,r}B_{j+1}^{n-1,r+1}B_j^{n-1,r+1}$, $(j,n,r) \in \Omega(B), j < J_b$ and $r < R$, are the BCEs in zone B; and (iii) rectangles $C_j^{n-1}C_{j+1}^{n-1}C_{j+1}^{n}C_j^{n}$, $(j,n) \in \Omega(C)$ and $j < J_c$, are the BCEs in zone C. Thus the BCEs are nonoverlapping and they can be used to fill the entire computational domain.

(b) Consider figure 3. For an interior grid point in zone A, say point A_1^1, both $\mathrm{CE}_+(A_1^1)$ and $\mathrm{CE}_-(A_1^1)$ are defined and they occupy rectangles $A_1^0\,A_2^0\,A_2^1\,A_1^1$ and $A_0^0\,A_1^0\,A_1^1\,A_0^1$, respectively. On the other hand, for a boundary grid point in zone A, say point A_2^1, only $\mathrm{CE}_-(A_2^1)$ is defined and it occupies rectangle $A_1^0A_2^0A_2^1A_1^1$ while $\mathrm{CE}_+(A_2^1)$ is undefined. Application of similar definitions to all grid zones leads to the conclusions that: (i) two BCE*s are assigned to each interior grid point of a grid zone while only one is assigned to a boundary grid point; and (ii) each BCE has two cohosts.

3.2 LTS procedure and its justification

To proceed, we begin with the following preliminaries:

(a) Three numerical analogues of u, $\partial u/\partial x$ and $\partial u/\partial t$, denoted by $u(G)$, $u_x(G)$ and $u_t(G)$, respectively, are assigned to each grid point G (which may represent any A_j^n, or $B_j^{n,r}$, or C_j^n). In addition, let (i)

$$\vec{h}^*(x,t;G) \equiv (au^*(x,t;G), u^*(x,t;G)) \tag{3.11}$$

$$u_t(G) \equiv -a\,u_x(G) \tag{3.12}$$

and

$$u^*(x,t;G) = u(G) + u_x(G) \times [(x - x(G)) - a(t - t(G))] \tag{3.13}$$

be the current versions of equations (2.4)–(2.6), respectively; and (ii)

$$\hat{u}_x\left(A_j^n\right) \equiv \frac{\Delta x}{2}u_x\left(A_j^n\right),$$
$$\hat{u}_x\left(B_j^{n,r}\right) \equiv \frac{\Delta x}{2R}u_x\left(B_j^{n,r}\right) \quad \text{and} \tag{3.14}$$
$$\hat{u}_x\left(C_j^n\right) \equiv \frac{\Delta x}{2}u_x\left(C_j^n\right)$$

Also, hereafter let the 2×1 column matrix with its first and second elements being $u(G)$ and $\hat{u}_x(G)$, respectively, be denoted by $\vec{q}(G)$.

(b) Let (i) $A_{J_a-1}^{n-1,r}$ (see figures 2 and 4) denote the point with

$$x = (J_a - 1)\Delta x \quad \text{and} \quad t = \left(n - 1 + \frac{r}{R}\right)\Delta t \tag{3.15}$$

(ii) $C_1^{n-1,r}$ (see figures 2 and 5) denote the point with

$$x = (M_2 + 1)\Delta x \quad \text{and} \quad t = \left(n - 1 + \frac{r}{R}\right)\Delta t \tag{3.16}$$

(iii) $u'(A_{J_a-1}^{n-1,r})$ denote the first-order Taylor's approximation of u at point $(A_{J_a-1}^{n-1,r})$, evaluated in terms of $\vec{q}(A_{J_a-1}^{n-1})$; and (iv) $u'(C_1^{n-1,r})$ denote the first-order Taylor's approximation of u at point $C_1^{n-1,r}$, evaluated in terms of $\vec{q}(C_1^{n-1})$. Then we have

$$u'\left(A_{J_a-1}^{n-1,r}\right) \equiv u\left(A_{J_a-1}^{n-1}\right) + \frac{r\Delta t}{R}u_t\left(A_{J_a-1}^{n-1}\right)$$
$$= u\left(A_{J_a-1}^{n-1}\right) - \frac{2r\nu}{R}\hat{u}_x\left(A_{J_a-1}^{n-1}\right) \tag{3.17}$$

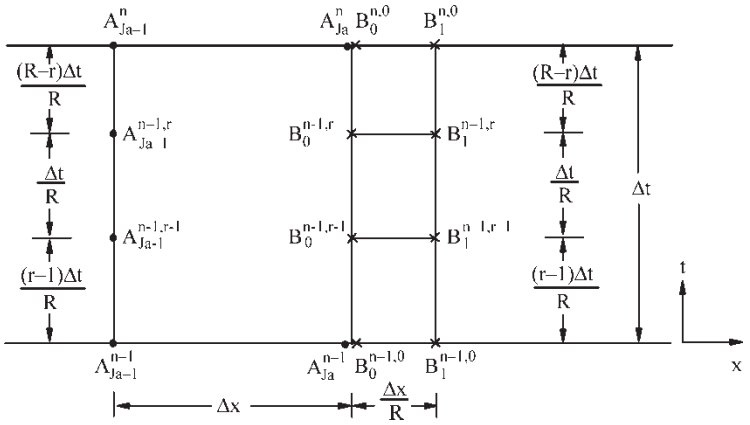

Figure 4. The grid points neighboring to the interface separating zones A and B ($R = 3$ and $r = 2$).

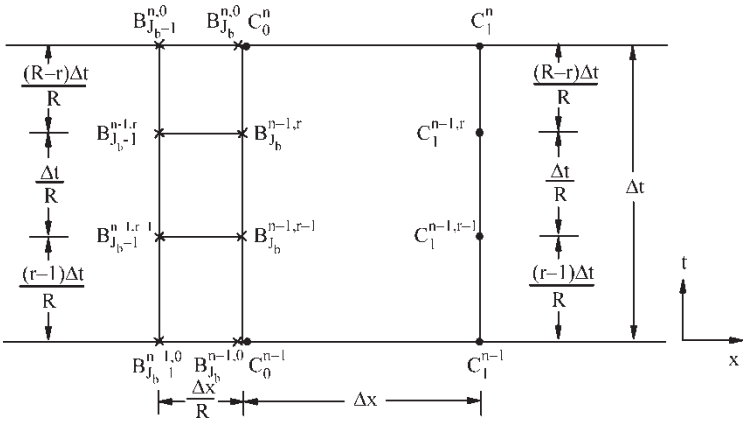

Figure 5. The grid points neighboring to the interface separating zones B and C ($R = 3$ and $r = 2$).

and

$$u'\left(C_1^{n-1,r}\right) \equiv u\left(C_1^{n-1}\right) + \frac{r\Delta t}{R} u_t\left(C_1^{n-1}\right) = u\left(C_1^{n-1}\right) - \frac{2r\nu}{R}\hat{u}_x\left(C_1^{n-1}\right) \quad (3.18)$$

The validity of the last equality sign in either equation (3.17) or (3.18) follows from equations (3.12) and (3.14), and $\nu \equiv a\Delta t/\Delta x$.

(c) Let (i) $u'(B_1^{n,0})$ be the first-order Taylor's approximation of u at point $B_1^{n,0}$, evaluated in terms of $\vec{q}(B_1^{n-1,R-1})$ (see figure 4); and (ii) $u'(B_{J_b-1}^{n,0})$ be the first-order Taylor's approximation of u at point $(B_{J_b-1}^{n,0})$, evaluated in terms of $\vec{q}(B_{J_b-1}^{n-1,R-1})$ (see figure 5). Then we have

$$u'\left(B_1^{n,0}\right) \equiv u\left(B_1^{n-1,R-1}\right) + \frac{\Delta t}{R} u_t\left(B_1^{n-1,R-1}\right) = u\left(B_1^{n-1,R-1}\right) - 2\nu\hat{u}_x\left(B_1^{n-1,R-1}\right) \quad (3.19)$$

and

$$u'\left(B_{J_b-1}^{n,0}\right) \equiv u\left(B_{J_b-1}^{n-1,R-1}\right) + \frac{\Delta t}{R} u_t\left(B_{J_b-1}^{n-1,R-1}\right) = u\left(B_{J_b-1}^{n-1,R-1}\right) - 2\nu\hat{u}_x\left(B_{J_b-1}^{n-1,R-1}\right) \quad (3.20)$$

(d) Let $\overline{PQ}$ be a face of a BCE* denoted by V (see figure 6). Let G be a grid point that may or may not coincide with point P or point Q. Then

$$I(\overline{PQ}; G; V) \equiv \int_{\overline{PQ}} \vec{h}^*(x,t;G)\cdot d\vec{s} \quad (3.21)$$

Here $d\vec{s} = d\sigma\vec{n}$ with (i) $d\sigma$ being the length of a differential element of $\overline{PQ}$; and (ii) $\vec{n}$ being the unit vector normal to $\overline{PQ}$ and pointing outward from V. Note that: (i) with the aid of equations (3.11), (3.13) and (3.21), $I(\overline{PQ}; G; V)$ *represents the I-flux leaving V through* $\overline{PQ}$ *and is evaluated using* $\vec{q}(G)$; and (ii) for simplicity, hereafter we adopt the abbreviation:

$$I(\overline{PQ}; V) \equiv I(\overline{PQ}; P; V) \quad (3.22)$$

Based on the above preliminaries, we now provide a step-by-step description of the current LTS that occurs between $t = (n-1)\Delta t$ and $t = n\Delta t$. It is then followed by an explanation of why the LTS procedure is so constructed. We consider only the case $n = 1$. The general case, however, can be constructed by simply replacing the coarse time level indices "0" and "1" with "$n-1$" and "n", respectively.

§1. Because $a > 0$, equation (2.1) models a convective process in which information propagates from left to right. As a result, we can assume that the initial data at $t = 0$ and the boundary data at $x = 0$ are given. Thus $\vec{q}(A_0^1)$ can be specified using the given left boundary data. On the other hand, $\vec{q}(C_{J_c}^1)$ can be evaluated using the boundary condition

$$\vec{q}(C_{J_c}^1) = \nu\vec{q}(C_{J_c-1}^0) + (1-\nu)\vec{q}(C_{J_c}^0) \quad (3.23)$$

which can be derived from the method of characteritics. Alternatively, one can assume that

$$\vec{q}(A_0^1) = \vec{q}(A_1^0) \text{ and } \vec{q}(C_{J_c}^1) = \vec{q}(C_{J_c-1}^0) \quad (3.24)$$

For the CESE method, the boundary conditions given in equation (3.24) are non-reflecting in nature (Chang *et al.* 2003) if (i) $u(x,0)$) based on which the grid initial data are specified) has a flat profile outside a bounded interval, i.e.

$$u(x,0) = \begin{cases} u_o(x_-), & \text{if } -\infty < x \le x_- \\ u_o(x), & \text{if } x_- < x < x_+ \\ u_o(x_+), & \text{if } x_+ \le x < +\infty \end{cases} \quad (3.25)$$

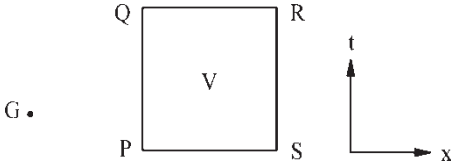

Figure 6. A point G and an edge $\overline{PQ}$ of a rectangle V.

where x_- and x_+ are given constants, and $u_o(x)$ is a given function; (ii) A_0^0 and A_0^1 lie on the left boundary of a uniform space-time grid zone that has a width $\geq 2\Delta x_-$, where Δx_- is the spatial grid size of this zone; (iii) $C_{J_c}^0$ and $C_{J_c}^1$ lie on the right boundary of a uniform space-time grid zone that has a width $\geq 2\Delta x_+$, where Δx_+ is the spatial grid size of this zone; and (iv)

$$x(A_0^0) + 2\Delta x_- \leq x_- < x_+ \leq x(C_{J_c}^0) - 2\Delta x_+ \qquad (3.26)$$

§2. Using the dual a-α scheme, (i) for each $j = 1, 2, 3, \ldots, j_a - 1$, $\vec{q}(A_j^1)$ is determined in terms of $\vec{q}(A_{j-1}^0)$ and $\vec{q}(A_{j+1}^0)$; and (ii) for each $j = 1, 2, 3, \ldots, J_c - 1$, $\vec{q}(C_j^1)$ is determined in terms of $\vec{q}(C_{j-1}^0)$ and $\vec{q}(C_{j+1}^0)$.

§3. Using the dual a-α scheme (with the understanding that Δx and Δt are replaced by $\Delta x/R$ and $\Delta t/R$, respectively), for each $r = 1, 2, 3, \ldots, R$ and each $j = 1, 2, 3, \ldots, J_b - 1$, $\vec{q}(B_j^{0,r})$ is determined in terms of $\vec{q}(B_{j-1}^{0,r-1})$ and $\vec{q}(B_{j+1}^{0,r-1})$. As an example, $\vec{q}(B_1^{0,1})$is determined in terms of $\vec{q}(B_0^{0,0})$ and $\vec{q}(B_2^{0,0})$ (see figure 3).

§4. For a reason to be given later, $\vec{q}(B_0^{0,r})$, $r = 1, 2, \ldots, R$, are updated using (see figure 4 with $n = 1$).

$$u(B_0^{0,r}) = \frac{1}{2R+1}u'(A_{J_a-1}^{0,r}) + \frac{2R}{2R+1}\left\{(1-\nu)[u-(1+\nu)\hat{u}_x](B_1^{0,r-1}) + \nu\left[u - \frac{(2r-1)\nu}{R}\hat{u}_x\right](A_{J_a}^0)\right\} \qquad (3.27)$$

and

$$\hat{u}_x(B_0^{0,r}) = \frac{1}{2R}\left[u(B_0^{0,r}) - u'(A_{J_a-1}^{0,r})\right] \qquad (3.28)$$

Note that:

(a) To simplify notation, hereafter we adopt a convention that can be explained using an expression on the right side of equation (3.27) as an example, i.e.

$$[u-(1+\nu)\hat{u}_x](B_1^{0,r-1}) \equiv u(B_1^{0,r-1}) - (1+\nu)\hat{u}_x(B_1^{0,r-1}) \qquad (3.29)$$

(b) Because $u'(A_{J_a-1}^{0,r})$ is a function of $\vec{q}(A_{J_a-1}^0)$ (see equation (3.17)), equations (3.27) and (3.28) imply that $\vec{q}(B_0^{0,r})$ is a function of $\vec{q}(A_{J_a-1}^0)$, $\vec{q}(A_{J_a}^0)$, and $\vec{q}(B_1^{0,r-1})$.

(c) By using equations (3.6), (3.8), (3.11), (3.13), (3.14), (3.21), and (3.22) and also Remark (a) given immediately following equation (2.11), one concludes that equations (3.27) and (3.28) follow from

$$u_x(B_0^{0,r}) = \frac{u(B_0^{0,r}) - u'(A_{J_a-1}^{0,r})}{\Delta x} \qquad (3.30)$$

and

$$I(\overline{B_0^{0,r-1}B_0^{0,r}}; A_{J_a}^0; V) + I(\overline{B_0^{0,r}B_1^{0,r}}; V) + I(\overline{B_1^{0,r-1}B_0^{0,r-1}}; V) + I(\overline{B_1^{0,r-1}B_1^{0,r}}; V) = 0 \qquad (3.31)$$

where $V \equiv \mathrm{CE}_+(B_0^{0,r})$. Equation (3.30) states that $u_x(B_0^{0,r})$ is equal to the finite-difference approximation of $\partial u/\partial x$ at $B_0^{0,r}$ evaluated from the left using $u(B_0^{0,r})$ and $u'(A_{J_a-1}^{0,r})$. On the other hand, equation (3.31) represents a flux conservation condition over $\mathrm{CE}_+(B_0^{0,r})$ involving only *I-fluxes*.

§5. For a reason to be given later, $\vec{q}(B_{J_b}^{0,r})$ $r = 1, 2, \ldots, R$, are updated using (see figure 5 with $n = 1$)

$$u(B_{J_b}^{0,r}) = \frac{1}{2R+1}u'(C_1^{0,r}) + \frac{2R}{2R+1}\left\{(1+\nu)[u+(1-\nu)\hat{u}_x](B_{J_b-1}^{0,r-1})) - \nu\left[u - \frac{(2r-1)\nu}{R}\hat{u}_x\right](C_0^0)\right\} \qquad (3.32)$$

and

$$\hat{u}_x(B_{J_b}^{0,r}) = \frac{1}{2R}\left[u'(C_1^{0,r}) - u(B_{J_b}^{0,r})\right] \qquad (3.33)$$

Note that:

(a) Because $u'(C_1^{0,r})$ is a function of $\vec{q}(C_1^0)$ (see equation (3.18)), equations (3.32) and (3.33) imply that $\vec{q}(B_{J_b}^{0,r})$ is a function of $\vec{q}(C_1^0)$, $\vec{q}(C_0^0)$ and $\vec{q}(B_{J_b-1}^{0,r-1})$.

(b) It can be shown that equations (3.32) and (3.33) follow from

$$u_x(B_{J_b}^{0,r}) = \frac{u'(C_1^{0,r}) - u(B_{J_b}^{0,r})}{\Delta x} \qquad (3.34)$$

and

$$I(\overline{B_{J_b}^{0,r-1}B_{J_b}^{0,r}}; C_0^0; V) + I(\overline{B_{J_b}^{0,r}B_{J_b-1}^{0,r}}; V) + I(\overline{B_{J_b-1}^{0,r-1}B_{J_b}^{0,r-1}}; V) + I(\overline{B_{J_b-1}^{0,r-1}B_{J_b-1}^{0,r}}; V) = 0 \qquad (3.35)$$

where $V \equiv \mathrm{CE}_-(B_{J_b}^{0,r})$. Equation (3.34) states that $u_x(B_{J_b}^{0,r})$ is equal to the finite-difference approximation of $\partial u/\partial x$ at $B_{J_b}^{0,r}$ evaluated from the right using $u'(C_1^{0,r})$ and $u(B_{J_b}^{0,r})$. On the other hand, equation (3.35) represents a flux conservation condition over $\mathrm{CE}_-(B_{J_b}^{0,r})$ involving only *I-fluxes*.

§6. For a reason to be given later, $\vec{q}(A_{J_a}^1)$ is updated using (see figure 4 with $n = 1$).

$$u(A_{J_a}^1) = \frac{R}{R+2}u'(B_1^{1,0}) + \frac{2(1+\nu)}{R+2}[u+(1-\nu)\hat{u}_x](A_{J_a-1}^0) - \frac{2\nu}{R(R+2)}\sum_{r=0}^{R-1}(u-\nu\hat{u}_x)(B_0^{0,r}) \qquad (3.36)$$

and

$$\hat{u}_x(A^1_{J_a}) = \frac{R}{2}\left[u'(B^{1,0}_1) - u(A^1_{J_a})\right] \tag{3.37}$$

Note that:

(a) Because $u'(B^{1,0}_1)$ is a function of $\vec{q}(B^{0,R-1}_1)$ (see equation (3.19)), equations (3.36) and (3.37) imply that $\vec{q}A^1_{J_a}$ is a function of $\vec{q}(B^{0,R-1}_1)$, $\vec{q}(A^0_{J_a-1})$, and $\vec{q}(B^{0,r}_0)$, $r = 0, 1, 2, \ldots, R-1$.

(b) It can be shown that equations (3.36) and (3.37) follow from

$$u_x(A^1_{J_a}) = \frac{u'(B^{1,0}_1) - u(A^1_{J_a})}{\Delta x/R} \tag{3.38}$$

and

$$\sum_{r=0}^{R-1} I(\overline{B^{0,r}_0(B^{0,r+1}_0}; V) + I(\overline{A^1_{J_a}A^1_{J_a-1}}; V) + I(\overline{A^0_{J_a-1}A^0_{J_a}}; V) + I(\overline{A^0_{J_a-1}A^1_{J_a-1}}; V) = 0 \tag{3.39}$$

where $V \equiv \mathrm{CE}_-(A^1_{J_a})$. Equation (3.38) states that $u_x(A^1_{J_a})$ is equal to the finite-difference approximation of $\partial u/\partial x$ at $(A^1_{J_a})$ evaluated from the right using $u'(\mathrm{B}^{1,0}_1)$ and $u(A^1_{J_a})$. On the other hand, equation (3.39) represents a flux conservation condition over $\mathrm{CE}_-(A^1_{J_a})$ involving only *I-fluxes*.

§7. For a reason to be given later, $\vec{q}(C^1_0)$ is updated using (see figure 5 with $n = 1$).

$$u(C^1_0) = \frac{R}{R+2}u'(B^{1,0}_{J_b-1}) + \frac{2(1-\nu)}{R+2}[u - (1+\nu)\hat{u}_x](C^0_1) + \frac{2\nu}{R(R+2)}\sum_{r=0}^{R-1}(u - \nu\hat{u}_x)(B^{0,r}_{J_b}) \tag{3.40}$$

and

$$\hat{u}_x(C^1_0) = \frac{R}{2}\left[u(C^1_0) - u'(B^{1,0}_{J_b-1})\right] \tag{3.41}$$

Note that:

(a) Because $u'(B^{1,0}_{J_b-1})$ is a function of $\vec{q}(B^{0,R-1}_{J_b-1})$ (see equation (3.20)), equations (3.40) and (3.41) imply that $\vec{q}(C^1_0)$ is a function of $\vec{q}(B^{0,R-1}_{J_b-1})$, $\vec{q}(C^0_1)$, and $\vec{q}(B^{0,r}_{J_b})$, $r = 0, 1, 2, \ldots, R-1$.

(b) It can be shown that equations (3.40) and (3.41) follow from

$$u_x(C^1_0) = \frac{u(C^1_0) - u'(B^{1,0}_{J_b-1})}{\Delta x/R} \tag{3.42}$$

and

$$\sum_{r=0}^{R-1} I(\overline{B^{0,r}_{J_b}B^{0,r+1}_{J_b}}; V) + I(\overline{C^1_0C^1_1}; V) + I(\overline{C^1_1C^0_0}; V) + I(\overline{C^0_1C^1_1}; V) = 0 \tag{3.43}$$

where $V \equiv \mathrm{CE}_+(C^1_0)$. Equation (3.42) states that $u_x(C^1_0)$ is equal to the finite-difference approximation of $\partial u/\partial x$ at C^1_0 evaluated from the left using $u(C^1_0)$ and $u'(B^{1,0}_{J_b-1})$. On the other hand, equation (3.43) represents a flux conservation condition over $\mathrm{CE}_+(C^1_0)$ involving only *I-fluxes*.

This concludes the description of the LTS procedure. In the following, using the grid structure depicted in figure 3 as an example, we will explain why the procedure is so constructed. In particular, it will be shown that the current construction results in a key conservation property, i.e. the D-flux is conserved over any space-time region that is the union of any combination of BCEs.

As a preliminary, the G-fluxes associated with the current grid structure are defined in the following remarks:

(a) Let $V \equiv \mathrm{CE}_+(A^1_0)$. By definition, the G-fluxes leaving V through $\overline{A^1_0A^1_1}$, $\overline{A^0_1A^0_0}$, and $\overline{A^0_1A^1_1}$ are $I(\overline{A^1_0A^1_1}; V)$, $I(\overline{A^0_1A^0_0}; V)$, and $I(\overline{A^0_1A^1_1}; V)$, respectively. In addition, the G-flux leaving V through $(\overline{A^1_0A^0_0})$(an A-flux) is the negative of the sum of those leaving through other faces. Thus the G-flux is conserved over $\mathrm{CE}_+(A^1_0)$.

(b) Let $V \equiv \mathrm{CE}_-(A^1_1)$. By definition, the G-fluxes leaving V through $\overline{A^1_1A^1_0}$, $\overline{A^0_0A^0_1}$,and $\overline{A^0_0A^1_0}$ are $I(\overline{A^1_1A^1_0}; V)$, $I(\overline{A^0_0A^0_1}; V)$ and $I(\overline{A^0_0A^1_0}; V)$, respectively. In addition, the G-flux leaving V through $(\overline{A^1_1A^0_1})$ (an A-flux) is the negative of the sum of those leaving through other faces. Thus the G-flux is conserved over $\mathrm{CE}_-(A^1_1)$.

(c) Let $V \equiv \mathrm{CE}_+(A^1_1)$. By definition, the G-fluxes leaving V through $\overline{A^1_1A^1_2}$, $\overline{A^0_2A^0_1}$, $\overline{B^{0,0}_0B^{0,1}_0}$ and $\overline{B^{0,1}_0B^{1,0}_0}$ are $I(\overline{A^1_1A^1_2}; V)$, $I(\overline{A^0_2A^0_1}; V)$, $I(\overline{B^{0,0}_0B^{0,1}_0}; A^0_2; V)$ and $I(\overline{B^{0,1}_0B^{1,0}_0}; A^0_2; V)$, respectively. In addition, the G-flux leaving V through $\overline{A^1_1A^0_1}$ (an A-flux) is the negative of the sum of those leaving through other faces. Thus the G-flux is conserved over $\mathrm{CE}_+(A^1_1)$. Furthermore, because points $B^{0,0}_0$ and $B^{1,0}_0$ coincide with points A^0_2 and A^1_2, respectively, equations (3.21) and (3.22) imply that

$$I(\overline{A^0_2A^1_2}; V) = I(\overline{B^{0,0}_0B^{0,1}_0}; A^0_2; V) + I(\overline{B^{0,1}_0B^{1,0}_0}; A^0_2; V). \tag{3.44}$$

As such the G-flux leaving V through $\overline{A^0_2A^1_2}$ (the union of $\overline{B^{0,0}_0B^{0,1}_0}$ and $\overline{B^{0,1}_0B^{1,0}_0}$) is $I(\overline{A^0_2A^1_2}; V)$.

(d) Let $V \equiv \mathrm{CE}_-(A^1_2)$. By definition, the G-fluxes leaving V through $\overline{A^1_2A^1_1}$, $\overline{A^0_1A^0_2}$, and $\overline{A^0_1A^1_1}$ are $I(\overline{A^1_2A^1_1}; V)$, $I(\overline{A^0_1A^0_2}; V)$, and $I(\overline{A^0_1A^1_1}; V)$, respectively. In addition, the G-fluxes leaving V through $\overline{B^{0,0}_0B^{0,1}_0}$ and $\overline{B^{0,1}_0B^{1,0}_0}$ are $I(\overline{B^{0,0}_0B^{0,1}_0}; V)$, $I(\overline{B^{0,1}_0B^{1,0}_0}; V)$, respectively. Equation (3.39) coupled with the above definitions implies that the G-flux is conserved over $\mathrm{CE}_-(A^1_2)$.

(e) Let $V \equiv \mathrm{CE}_+(B^{0,1}_0)$. By definition, the G-fluxes leaving V through $(\overline{B^{0,1}_0B^{0,1}_1})$, $(\overline{B^{0,0}_1B^{0,0}_0})$, $(\overline{B^{0,0}_1B^{0,1}_1})$,

and $\overline{(B_0^{0,0}B_0^{0,1})}$ are $I(\overline{B_0^{0,1}B_1^{0,1}};V), I(\overline{B_1^{0,0}B_0^{0,0}};V)$, $I(\overline{B_1^{0,0}B_1^{0,1}};V)$, and $I(\overline{B_0^{0,0}B_0^{0,1}};A_2^0;V)$, respectively. Equation (3.31) coupled with the above definitions implies that the G-flux is conserved over $\mathrm{CE}_+(B_0^{0,1})$.

(f) Let $V \equiv \mathrm{CE}_+(B_0^{1,0})$. By definition, the G-fluxes leaving V through $\overline{B_0^{1,0}B_1^{1,0}}$, $\overline{B_1^{0,1}B_0^{0,1}}$, $\overline{B_1^{0,1}B_1^{1,0}}$, and $\overline{B_0^{0,1}B_0^{1,0}}$, are $I(\overline{B_0^{1,0}B_1^{1,0}};V), I(\overline{B_1^{0,1}B_0^{0,1}};V), I(\overline{B_1^{0,1}B_1^{1,0}};V)$, and $I(\overline{B_0^{0,1}B_1^{1,0}};A_2^0;V)$, respectively. Because (i) for each j, $B_j^{n-1,R}$ and $B_j^{n,0}$ represent the same grid point, and (ii) $n = 1$ and $R = 2$ are assumed in figure 3, equation (3.31) coupled with the above definitions implies that the G-flux is conserved over $\mathrm{CE}_+(B_0^{1,0})$.

(g) Let $V \equiv \mathrm{CE}_-(B_1^{0,1})$. By definition, the G-fluxes leaving V through $\overline{B_1^{0,1}B_0^{0,1}}$, $\overline{B_0^{0,0}B_1^{0,1}}$, and $\overline{B_0^{0,0}B_0^{0,1}}$ are $I(B_1^{0,1}B_0^{0,1};V), I(\overline{B_0^{0,0}B_1^{0,0}};V)$ and $I(\overline{B_0^{0,0}B_0^{0,1}};V)$, respectively. In addition, the G-flux leaving $\mathrm{CE}_-(B_1^{0,1})$ through $\overline{B_1^{0,1}B_1^{0,0}}$ (an A-flux) is the negative of the sum of those leaving through other faces. Thus the G-flux is conserved over $\mathrm{CE}_-(B_1^{0,1})$.

(h) Let $V \equiv \mathrm{CE}_-(B_1^{1,0})$. By definition, the G-fluxes leaving V through $\overline{B_1^{1,0}B_0^{1,0}}$, $\overline{B_0^{0,1}B_1^{0,1}}$, and $\overline{B_0^{0,1}B_0^{1,0}}$ are $I(\overline{B_1^{1,0}B_0^{1,0}};V)$, $I(\overline{B_0^{0,1}B_1^{0,1}};V)$, and $I(\overline{B_0^{0,1}B_0^{1,0}};V)$, respectively. In addition, the G-flux leaving $\mathrm{CE}_-(B_1^{1,0})$. through $\overline{(B_1^{1,0}B_1^{0,1})}$ (an A-flux) is the negative of the sum of those leaving through other faces. Thus the G-flux is conserved over $\mathrm{CE}_-(B_1^{1,0})$.

(i) The G-fluxes associated with $\mathrm{CE}_-(C_2^1)$, $\mathrm{CE}_+(C_1^1)$, $\mathrm{CE}_-(C_1^1)$, $\mathrm{CE}_+(C_0^1)$, $\mathrm{CE}_-(B_2^{0,1})$, $\mathrm{CE}_-(B_2^{1,0})$, $\mathrm{CE}_+(B_1^{0,1})$, and $\mathrm{CE}_+(B_1^{1,0})$ are similarly defined. Using equations (3.35) and (3.43), one concludes that the G-flux is conserved over each of above BCE*s.

The G-fluxes associated with the BCE*s that lie between any pair of consecutive time levels are defined in a way identical to that described above. As such the G-flux is conserved over all BCE*s. Moreover, because (i) each BCE are occupied by two BCE*s (i.e. there are two different sets of conserving G-fluxes defined at the boundary of each BCE), and (ii) the D-flux at any face of a BCE is defined to be the simple average of the two G-fluxes defined there, it follows that the D-flux is conserved over each BCE. As such, to show that the D-flux is conserved over the union of any combination of BCEs, one needs only to show that the D-flux leaving one of any two neighboring BCEs through their interface is the negative of that leaving the other BCE through the same face.

To proceed, consider $\overline{A_1^0A_1^1}$, a vertical interface in the interior of zone A. By definition, the G-fluxes leaving $\mathrm{CE}_+(A_0^1)$ and $\mathrm{CE}_-(A_2^1)$ through $\overline{A_1^0A_1^1}$ are $I(\overline{A_1^0A_1^1};\mathrm{CE}_+(A_0^1))$ and $I(\overline{A_1^0A_1^1};\mathrm{CE}_-(A_2^1))$, respectively (see items (a) and (d) above). Because the unit vector normal to $\overline{A_1^0A_1^1}$ and pointing outward from $\mathrm{CE}_+(A_0^1)$ is the negative of that normal to $\overline{A_1^0A_1^1}$ and pointing outward from $\mathrm{CE}_-(A_2^1)$, equations (3.21) and (3.22) imply that

$$I(\overline{A_1^0A_1^1};\mathrm{CE}_+(A_0^1)) + I(\overline{A_1^0A_1^1};\mathrm{CE}_-(A_2^1)) = 0 \tag{3.45}$$

Moreover, by definition, the G-fluxes leaving $\mathrm{CE}_-(A_1^1)$ and $\mathrm{CE}_+(A_1^1)$ through $\overline{A_1^1A_1^0}$ are the A-fluxes

$$\begin{aligned} A(\overline{A_1^1A_1^0};\mathrm{CE}_-(A_1^1)) \equiv -[&I(\overline{A_1^1A_0^1};\mathrm{CE}_-(A_1^1)) \\ &+ I(\overline{A_0^0A_1^0};\mathrm{CE}_-(A_1^1)) \\ &+ I(\overline{A_0^0A_0^1};\mathrm{CE}_-(A_1^1))] \end{aligned} \tag{3.46}$$

and

$$\begin{aligned} A(\overline{A_1^1A_1^0};\mathrm{CE}_+(A_1^1)) \equiv -[&I(\overline{A_1^1A_2^1};\mathrm{CE}_+(A_1^1)) \\ &+ I(\overline{A_2^0A_1^0};\mathrm{CE}_+(A_1^1)) \\ &+ I(\overline{A_2^0A_2^1};\mathrm{CE}_+(A_1^1))] \end{aligned} \tag{3.47}$$

respectively (see items (b) and (c) above). Because $\vec{q}(A_1^1)$ is evaluated in terms of $\vec{q}(A_0^0)$ and $\vec{q}(A_2^0)$ using the a-α scheme, one has the conservation condition

$$\oint_{S(\mathrm{CE}(A_1^1))} \vec{h}^* \cdot \mathrm{d}\vec{s} = 0 \tag{3.48}$$

Equation (3.48) implies that the sum of the six *I-fluxes* in the brackets on the right side of equations (3.46) and (3.47) vanishes. Thus it follows from equations (3.46) and (3.47) that

$$A(\overline{A_1^1A_1^0};\mathrm{CE}_-(A_1^1)) + A(\overline{A_1^1A_1^0};\mathrm{CE}_+(A_1^1)) = 0 \tag{3.49}$$

Because $\mathrm{CE}_+(A_0^1)$ and $\mathrm{CE}_-(A_1^1)$ occupy the same rectangle $A_0^0A_1^0A_1^1A_0^1$ while $\mathrm{CE}_-(A_2^1)$ and $\mathrm{CE}_+(A_1^1)$ occupy the same rectangle $A_1^0A_2^0A_2^1A_1^1$, the D-fluxes leaving the BCEs (rectangles) $A_0^0A_1^0A_1^1A_0^1$ and $A_1^0A_2^0A_2^1A_1^1$ through $A_1^1A_1^0$, by definition, are

$$\left[I(\overline{A_1^0A_1^1};\mathrm{CE}_+(A_0^1)) + A(\overline{A_1^1A_1^0};\mathrm{CE}_-(A_1^1))\right]/2 \tag{3.50}$$

and

$$\left[I(\overline{A_1^0A_1^1};\mathrm{CE}_-(A_2^1)) + A(\overline{A_1^1A_1^0};\mathrm{CE}_+(A_1^1))\right]/2 \tag{3.51}$$

respectively. It follows from equations (3.45) and (3.49) that the above two D-fluxes are the negative of each other. By applying similar arguments, one concludes that, for any two neighboring BCEs that are in the same grid zone and share a vertical interface, the D-flux leaving one of these BCEs through the interface is the negative of that leaving the other BCE through the same face.

Next consider $B_0^{0,0}B_0^{0,1}$, a vertical interface separating two BCEs in zones A and B, respectively. By definition, the G-fluxes leaving $\mathrm{CE}_+(A_1^1)$ and $\mathrm{CE}_+(B_0^{0,1})$ through $\overline{B_0^{0,0}B_0^{0,1}}$

are $I(\overline{B_0^{0,0}B_0^{0,1}}; A_2^0; \mathrm{CE}_+(A_1^1))$ and $I(\overline{B_0^{0,0}B_0^{0,1}}; A_2^0; \mathrm{CE}_+(B_0^{0,1}))$, respectively (see items (c) and (e) above). Moreover, the G-fluxes leaving $\mathrm{CE}_-(A_2^1)$ and $\mathrm{CE}_-(B_1^{0,1})$ through $\overline{B_0^{0,0}B_0^{0,1}}$ are $I(\overline{B_0^{0,0}B_0^{0,1}}; \mathrm{CE}_-(A_2^1))$ and $I(\overline{B_0^{0,0}B_0^{0,1}}; \mathrm{CE}_-(B_1^{0,1}))$, respectively (see items (d) and (g) above). Because the unit vector normal to $\overline{B_0^{0,0}B_0^{0,1}}$ and pointing outward from the BCE $A_1^0A_2^0A_2^1A_1^1$ (which are occupied by both $\mathrm{CE}_+(A_1^1)$ and $\mathrm{CE}_-(A_2^1)$) is the negative of that normal to $\overline{B_0^{0,0}B_0^{0,1}}$ and pointing outward from the BCE $B_0^{0,0}B_1^{0,0}B_1^{0,1}B_0^{0,1}$ (which are occupied by both $\mathrm{CE}_+(B_0^{0,1})$ and $\mathrm{CE}_-(B_1^{0,1})$), equations (3.21) and (3.22) imply that

$$I(\overline{B_0^{0,0}B_0^{0,1}}; A_2^0; \mathrm{CE}_+(A_1^1)) + I(\overline{B_0^{0,0}B_0^{0,1}}; A_2^0; \mathrm{CE}_+(B_0^{0,1})) = 0 \quad (3.52)$$

and

$$I(\overline{B_0^{0,0}B_0^{0,1}}; \mathrm{CE}_-(A_2^1)) + I(\overline{B_0^{0,0}B_0^{0,1}}; \mathrm{CE}_-(B_1^{0,1})) = 0 \quad (3.53)$$

i.e. the two fluxes that appear in equation (3.52) or equation (3.53) are really the two values of the same *I-flux* measured in two opposite directions. By using equations (3.52) and (3.53), one concludes that the two D-fluxes leaving the BCEs $A_1^0A_2^0A_2^1A_1^1$ and $B_0^{0,0}B_1^{0,0}B_1^{0,1}B_0^{0,1}$ through $\overline{B_0^{0,0}B_0^{0,1}}$ i.e.

$$\left[I(\overline{B_0^{0,0}B_0^{0,1}}; A_2^0; \mathrm{CE}_+(A_1^1)) + I(\overline{B_0^{0,0}B_0^{0,1}}; \mathrm{CE}_-(A_2^1))\right]/2 \quad (3.54)$$

and

$$\left[I(\overline{B_0^{0,0}B_0^{0,1}}; A_2^0; \mathrm{CE}_+(B_0^{0,1})) + I(\overline{B_0^{0,0}B_0^{0,1}}; \mathrm{CE}_-(B_1^{0,1}))\right]/2 \quad (3.55)$$

are the negative of each other. By applying similar arguments, one concludes that, for any two neighboring BCEs that are in different grid zones and share a vertical interface, the D-flux leaving one of these BCEs through the interface is the negative of that leaving the other BCE through the same face.

Next consider $\overline{A_1^1A_2^1}$, a horizontal interface separating two BCEs in zone A. By definition, the G-fluxes leaving $\mathrm{CE}_+(A_1^1)$ and $\mathrm{CE}_-(A_2^1)$ through $\overline{A_1^1A_2^1}$ are $I(\overline{A_1^1A_2^1}; \mathrm{CE}_+(A_1^1))$ and $I(\overline{A_2^1A_1^1}; \mathrm{CE}_-(A_2^1))$, respectively (see items (c) and (d) above). Because $\mathrm{CE}_+(A_1^1)$ and $\mathrm{CE}_-(A_2^1)$ occupy the same BCE $A_1^0A_2^0A_2^1A_1^1$, by definition, the D-flux leaving the BCE through $\overline{A_1^1A_2^1}$ is

$$\left[I(\overline{A_1^1A_2^1}; \mathrm{CE}_+(A_1^1)) + I(\overline{A_2^1A_1^1}; \mathrm{CE}_-(A_2^1))\right]/2 \quad (3.56)$$

Similarly, it can be shown that the D-flux leaving the BCE $A_1^1A_2^1A_2^2A_1^2$ (which sits right above the BCE $A_1^0A_2^0A_2^1A_1^1$ and is occupied by both $\mathrm{CE}_-(A_2^2)$ and $\mathrm{CE}_+(A_1^2)$) is

$$\left[I(\overline{A_1^1A_2^1}; \mathrm{CE}_-(A_2^2)) + I(\overline{A_2^1A_1^1}; \mathrm{CE}_+(A_1^2))\right]/2 \quad (3.57)$$

Because the unit vector normal to $\overline{A_1^1A_2^1}$ and pointing outward from the BCE $A_1^0A_2^0A_2^1A_1^1$ is the negative of that normal to $\overline{A_1^1A_2^1}$ and pointing outward from the BCE $A_1^1A_2^1A_2^2A_1^2$, equations (3.21) and (3.22) imply that the two D-fluxes given in equations (3.56) and (3.57) are the negative of each other. By applying similar arguments, one concludes that, for any two neighboring BCEs that are in the same grid zone and share a horizontal interface, the D-flux leaving one of these BCEs through the interface is the negative of that leaving the other BCE through the same face.

It has been shown that the D-flux leaving one of any two neighboring BCEs through their interface is the negative of that leaving the other BCE through the same face. This coupled with the established fact that the D-flux is conserved over each BCE implies that the D-flux is conserved over the union of any combination of BCEs.

Aside from preserving the above conservation property, as will be shown immediately, the current explicit LTS performed along an interface separating two grid zones of different time-step sizes is also designed to maintain scheme stability and facilitate information transfer across the interface and yet use only the smallest stencil possible.

As an example, consider the time stepping performed along $\overline{A_2^0A_2^1}$. According to steps §3, §4, and §6 of the LTS procedure presented earlier, (i) $\vec{q}(B_0^{0,1})$ is evaluated in terms of $\vec{q}(A_1^0)$, $\vec{q}(A_2^0)$, and $\vec{q}(B_1^{0,0})$, (ii) $\vec{q}(B_0^{1,0})$ is evaluated in terms of $\vec{q}(A_1^0)$, $\vec{q}(A_2^0)$, and $\vec{q}(B_1^{0,1})$, (iii) $\vec{q}(A_2^1)$ is evaluated in terms of $\vec{q}(B_1^{0,1})$, $\vec{q}(B_0^{0,1})$, $\vec{q}(B_0^{0,0})$, and $\vec{q}(A_1^0)$, and (iv) $\vec{q}(B_1^{0,1})$ is evaluated in terms of $\vec{q}(B_0^{0,0})$ and $\vec{q}(B_2^{0,0})$. Moreover, by combining the fact presented above, one also concludes that (i) $\vec{q}(B_0^{1,0})$ is a function of $\vec{q}(A_1^0)$, $\vec{q}(A_2^0)$, $\vec{q}(B_0^{0,0})$, and $\vec{q}(B_2^{0,0})$; and (ii) $\vec{q}(A_2^1)$ is a function of $\vec{q}(A_1^0)$, $\vec{q}(A_2^0)$, $\vec{q}(B_0^{0,0})$, $\vec{q}(B_1^{0,0})$, and $\vec{q}(B_2^{0,0})$. As such, the numerical domains of dependence for $\vec{q}(B_0^{0,1})$, $\vec{q}(B_0^{1,0})$, and $\vec{q}(A_2^1)$ at $t = 0$ are $\overline{A_1^0B_1^{0,0}}$, $\overline{A_1^0B_2^{0,0}}$, and $\overline{A_1^0B_2^{0,0}}$, respectively. Because each of $\overline{A_1^0B_1^{0,0}}$ and $\overline{A_1^0B_2^{0,0}}$ is the union of two finite domains in zones A and B, respectively, by adjusting Δt for either the advection speed $a \geq 0$ or $a \leq 0$, one can fulfill the stability requirement that the analytical domain of dependence must be a subset of the numerical domain of influence. As such, the current LTS procedure can be extended to simulate Euler flows in which information may propagate in all directions.

This section is concluded with the following remarks:

(a) Based on the fact that these procedures are constructed in such a manner that the analytical domain always falls within the numerical domain if the CFL number <1, and also on the results of

numerical experiments, it is concluded that the current LTS procedure and its Euler extensions generally are stable if (i) the CFL number < 1 for all space-time grid cells in all grid zones, and (ii) $\alpha \geq 1$. Also, these LTS procedures generally become more dissipative as α increases and the CFL number decreases. To prevent excessive local numerical dissipation, it is desirable that, by adjusting local time-step size, the CFL number be kept above some bound (say 0.3) for all grid cells. It is expected that the above general criteria is applicable even in the 2D and 3D cases to be discussed below.

(b) In a 2D CESE solver, each analytical variable u is associated with three grid variables u^n_{jk}, $(u_x)^n_{jk}$, and $(u_y)^n_{jk}$ at each "solution point" (j, k, n) (Chang *et al.* 1999, Wang and Chang 1999a, Zhang *et al.* 2002). The spatial grid can be generated from triangles (Chang *et al.* 1999, Wang and Chang 1999a) or quadrilaterals (Zhang *et al.* 2002). For a standard solver with a triangle-based (quardrilateral-based) spatial grid and a spatially independent time-step, each interior solution point is associated with three (four) BCEs. Moreover, regardless of whether the spatial grid is generated from triangles or quadrilaterals, each BCE is a space-time cylinder with the top and bottom faces being quadrilaterals. As such, at each time level, an interior solution point is associated with three or four quadrilaterals (in fact, the solution point associated with the common vertex of these quadrilaterals is the centroid of the union of the same quadrilaterals). Note that: (i) for a nonuniform spatial grid, a solution point generally does not coincide with the commom vertex of the associated quadrilaterals; and (ii) concepts similar to the I-, A-, G-, and D-fluxes were introduced in the 2D cases (Wang and Chang 1999a, Zhang *et al.* 2002) *albeit* that different terms are used (in fact, the generalized flux and the dual flux defined here were referred to as the modified flux and the generalized flux there, respectively).

Based on the above description, the 1D CESE LTS procedure described above can be easily extended to become its 2D version. Specifically, (i) interior solution points of a grid zone of uniform time-step size are defined using the definition given in (Wang and Chang 1999a); (ii) for the top or bottom face (which is a quadrilateral) of each boundary BCE of a grid zone of uniform time-step size, one of its vertices is associated with an interior solution point while the one facing the first vertex is designated as an exterior solution point of this grid zone; (iii) solution points with the same space-time location but belonging to grid zones of different time-step sizes are again assigned with independent sets of grid variables; (iv) the unknowns at an interior solution point of a grid zone can be evaluated using the 2D dual a–α scheme (Chang *et al.* 1999); and (v) the three unknowns at an exterior solution point are determined using an I-flux conservation condition (the counterpart to the 1D condition such as equation (3.31)) and two finite-difference conditions (the counterparts to the 1D condition such as equation (3.30)) that provide the grid analogues of u_x and u_y. Note that, other than it must involve at least three different grid values of u, construction of the grid analogues of u_x and u_y has a high degree of freedom. However, to maintain stability and facilitate information transfer across the interface without incurring excessive numerical dissipation, the analogues should be constructed with a minimum stencil and yet using the information from all grid zones converging on the interface grid point under consideration.

(c) In a 3D CESE solver, each analytical variable u is associated with four grid variables at each solution point (Wang and Chang 1999a, Zhang *et al.* 2002). The spatial grid can be generated from tetrahedrons (Wang and Chang 1999a) or hexahedrons (Zhang *et al.* 2002). For a standard solver with a tetrahedron-based (hexahedron-based) spatial grid and a spatially independent time-step, each interior solution point is associated with four (six) BCEs. *Albeit* it is more complex, nevertheless a 3D version of the current 1D LTS procedure can be built using the guidelines similar to those provided for the construction of a 2D LTS procedure.

(d) Because the spatial grid structures used in the LTS procedures described above are fixed in time, these procedures cannot be used in simulations in which accuracy consideration requires that spatial fine-grid zones be moved with time (how they are moved with time is a subject beyond the present work—here it is simply assumed that at some time level, say $t = t^n$, a reconstructed spatial grid with a new grid point distribution is given). This limitation, however, can be overcome if the LTS procedures are complemented by the spatial grid value reconstruction procedures to be described in section 4.

4. Spatial grid value reconstruction

As a preliminary, consider any set of grid points $G_0, G_1, G_2, \ldots, G_K$ which lie on the time level $t = t^n$ and satisfy

$$x(G_0) < x(G_1) < x(G_2) < \cdots < x(G_K) \tag{4.1}$$

Here (i) $t = t^n$ represents a common time level of all space-time grid zones, and (ii) $x(P)$ denotes the x-coordinate of any point P. Let (i) k be any integer with

$0 \le k < K$, (ii) P_k and P'_k be two points with $t = t^n$ and

$$x(G_k) \le x(P_k) \le x(P'_k) \le x(G_{k+1}), \tag{4.2}$$

and (iii) V^n be the space-time region $t < t^n$. Then, according to the definitions given earlier, the D-flux leaving V^n through $\overline{P_k P'_k}$ is

$$D(\overline{P_k P'_k}; G_k, G_{k+1}; V^n) \equiv \frac{1}{2}\left[I(\overline{P_k P'_k}; G_k; V^n) + I(\overline{P_k P'_k}; G_{k+1}; V^n)\right] \tag{4.3}$$

Here, for any points P, Q, and G lying on the time level $t = t^n$,

$$I(\overline{PQ}; G; V^n) = \int_{\min\{x(P),x(Q)\}}^{\max\{x(P),x(Q)\}} u^*(x, t^n; G)\mathrm{d}x \tag{4.4}$$

Obviously equation (4.4) follows from equation (3.11) and (3.21).

Moreover, for a line segment with $t = t^n$ and not being bounded by two neighboring grid points, the D-flux leaving V^n through the line segment can be defined in terms of the component D-fluxes defined in equation (4.3). As an example, let P and Q be two points with $t = t^n$ and

$$x(G_0) \le x(P) < x(G_1) < x(Q) \le x(G_2) \tag{4.5}$$

Then, by definition, the D-flux leaving V^n through $\overline{PQ}$ is

$$D(\overline{PQ}; G_0, G_2; V^n) \equiv D(\overline{PG_1}; G_0, G_1; V^n) + D(\overline{G_1 Q}; G_1, G_2; V^n) \tag{4.6}$$

For simplicity, hereafter we adopt the abbreviation:

$$D(\overline{PQ}; V^n) \equiv D(\overline{PQ}; P, Q; V^n) \tag{4.7}$$

According to equations (3.21) and (3.22), the I-flux $I(\overline{PQ}; V^n)$ is only a function of $\vec{q}(P)$. On the other hand, according to equations (4.3), (4.4), (4.6), and (4.7), the D-flux $D(\overline{PQ}; V^n)$ is a function of the set $\{\vec{q}\}$ associated with the grid points P and Q and all the grid points sandwiched between P and Q.

With the above preparations, the essence of the current spatial grid value reconstruction (SGVR) procedure will be described using figure 7 where the given "original" and "reconstructed" spatial grids at $t = t^n$ are depicted. In each grid, a uniform spatial fine-grid zone B is sandwiched between two uniform spatial coarse-grid zones A and C. Moreover we assume that

$$x(A_0) = x(A'_0) = 0 \tag{4.8}$$

$$x(A_1) = x(B_0) = x(A'_1) = \Delta x \tag{4.9}$$

$$x(B_1) = (3/2)\Delta x \tag{4.10}$$

$$x(B_2) = x(A'_2) = x(B'_0) = 2\Delta x \tag{4.11}$$

$$x(B_3) = x(B'_1) = (5/2)\Delta x \tag{4.12}$$

$$x(B_4) = x(C_0) = x(B'_2) = 3\Delta x \tag{4.13}$$

$$x(B'_3) = (7/2)\Delta x \tag{4.14}$$

$$x(C_1) = x(B'_4) = x(C'_0) = 4\Delta x \tag{4.15}$$

$$x(C_2) = x(C'_1) = 5\Delta x \tag{4.16}$$

It follows from equations (4.8)–(4.16) that, in either the original or the reconstructed grid, two neighboring grid points in zone A or C is separated by a distance Δx while two neighboring grid points in zone B is separated by a distance $\Delta x' = \Delta x/2$.

In the current development, the set of the grid values $\{\vec{q}\}$ of the reconstructed grid points (see figure 7b) will be evaluated in terms of the set of the known grid values $\{\vec{q}\}$ of the original grid points (see figure 7a) in a manner that is consistent with a D-flux conservation condition, i.e. the D-flux leaving V^n through any *reconstructed* grid interval evaluated using the reconstructed $\{\vec{q}\}$ is identical to that evaluated using the known original $\{\vec{q}\}$. The above condition by no means implies that the D-flux leaving V^n through any *original* grid interval evaluated using the original $\{\vec{q}\}$ is identical to that evaluated using the reconstructed $\{\vec{q}\}$. Thus, in the current development, the D-flux is generally not conserved over a space-time region that is the union of a combination of BCEs unless each interface that splits the region into two with one being above and another below a reconstruction time level is the union of *reconstructed* grid intervals.

Also, by no means, the above imposed D-flux conservation condition provides an unique solution of the "reconstructed" $\{\vec{q}\}$ in terms of the known "original" $\{\vec{q}\}$. In the following, we describe two of the simplest procedures by which the "reconstructed" $\{\vec{q}\}$ can be uniquely determined.

With the aid of equations (4.4) and (3.22), the first SGVR procedure is specified using the following rules:

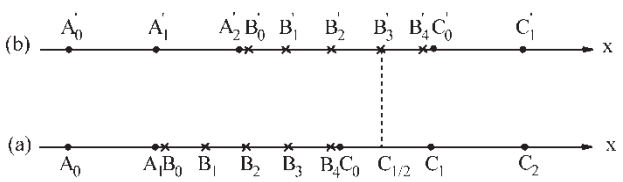

Figure 7. (a) The original grid points, and (b) the reconstructed grid points, at the time level $t = t^n$.

§1. No reconstruction of grid values is required for the end grid points A_0' and C_1', i.e.

$$\vec{q}(A_0') = \vec{q}(A_0) \text{ and } \vec{q}(C_1') = \vec{q}(C_2) \tag{4.17}$$

As such, we have

$$I(\overline{A_0'A_1'}; V^n) = I(\overline{A_0A_1}; V^n) \tag{4.18}$$

and

$$I(\overline{C_1'C_0'}; V^n) = I(\overline{C_2C_1}; V^n) \tag{4.19}$$

§2. $\vec{q}(A_1')$ is determined in terms of $\vec{q}(A_1)$, $\vec{q}(B_0)$, and $\vec{q}(B_1)$ by assuming

$$I(\overline{A_1'A_0'}; V^n) = I(\overline{A_1A_0}; V^n) \tag{4.20}$$

and

$$I(\overline{A_1'A_2'}; V^n) = I(\overline{B_0B_1}; V^n) + I(\overline{B_1B_2}; V^n) \tag{4.21}$$

§3. $\vec{q}(A_2')$ is determined in terms of $\vec{q}(B_1), \vec{q}(B_2)$, and $\vec{q}(B_1')$ by assuming

$$I(\overline{A_2'A_1'}; V^n) = I(\overline{B_2B_1}; V^n) + I(\overline{B_1B_0}; V^n) \tag{4.22}$$

and

$$u_x(A_2') = \frac{u(B_1') - u(A_2')}{\Delta x'} \tag{4.23}$$

Note that, according to §5, $\vec{q}(B_1') = \vec{q}(B_3)$.

§4. $\vec{q}(B_0')$ is determined in terms of $\vec{q}(B_2)$ and $\vec{q}(A_1')$ by assuming

$$I(\overline{B_0'B_1'}; V^n) = I(\overline{B_2B_3}; V^n) \tag{4.24}$$

and

$$u_x(B_0') = \frac{u(B_0') - u(A_1')}{\Delta x} \tag{4.25}$$

§5. $\vec{q}(B_1')$ is determined by assuming

$$I(\overline{B_1'B_0'}; V^n) = I(\overline{B_3B_2}; V^n) \tag{4.26}$$

and

$$I(\overline{B_1'B_2'}; V^n) = I(\overline{B_3B_4}; V^n) \tag{4.27}$$

In fact, equations (4.26) and (4.27) imply that $\vec{q}(B_1') = \vec{q}(B_3')$.

§6. $\vec{q}(B_2')$ is determined in terms of $\vec{q}(B_4')$ and $\vec{q}(C_0)$ by assuming

$$I(\overline{B_2'B_1'}; V^n) = I(\overline{B_4B_3}; V^n) \tag{4.28}$$

and

$$I(\overline{B_2'B_3'}; V^n) = I(\overline{C_0C_{1/2}}; V^n) \tag{4.29}$$

where $C_{1/2}$ is a point with $t = t^n$ and $x(C_{1/2}) = x(B_3')$.

§7. $\vec{q}(B_3')$ is determined in terms of $\vec{q}(C_0)$ and $\vec{q}(C_1)$ by assuming

$$I(\overline{B_3'B_2'}; V^n) = I(\overline{C_0C_{1/2}}; C_1; V^n) \tag{4.30}$$

and

$$I(\overline{B_3'B_4'}; V^n) = I(\overline{C_{1/2}C_1}; C_0; V^n) \tag{4.31}$$

§8. $\vec{q}(B_4')$ is determined in terms of $\vec{q}(C_1)$ and $\vec{q}(C_1')$ by assuming

$$I(\overline{B_4'B_3'}; V^n) = I(\overline{C_1C_{1/2}}; V^n) \tag{4.32}$$

and

$$u_x(B_4') = \frac{u(C_1') - u(B_4')}{\Delta x} \tag{4.33}$$

§9. $\vec{q}(C_0')$ is determined in terms of $\vec{q}(C_1)$ and $\vec{q}(B_3')$ by assuming

$$I(\overline{C_0'C_1'}; V^n) = I(\overline{C_1C_2}; V^n) \tag{4.34}$$

and

$$u_x(C_0') = \frac{u(C_0') - u(B_3')}{\Delta x'} \tag{4.35}$$

With the aid of equations (4.1)–(4.16) and (3.22), equations (4.18)–(4.22), (4.24), (4.26)–(4.32), and (4.34) imply that the reconstructed $\{\vec{q}\}$ does indeed satisfy the D-flux conservation condition if it is specified according to the above SGVR procedure.

With the aid of equations (4.3)–(4.7), and (3.22), the second SGVR procedure is specified using the following rules:

§1. $\vec{q}(A_0')$ is detemined in terms of $\vec{q}(A_0)$ and $\vec{q}(A_1)$ by assuming

$$u(A_0') = u(A_0) \tag{4.36}$$

and

$$I(\overline{A_0'A_1'}; V^n) = D(\overline{A_0A_1}; V^n) \tag{4.37}$$

§2. $\vec{q}(A_1')$ is determined in terms of $\vec{q}(A_0)$, $\vec{q}(A_1)$, $\vec{q}(B_0)$, $\vec{q}(B_1)$, and $\vec{q}(B_2)$ by assuming

$$I(\overline{A_1'A_0'}; V^n) = D(\overline{A_0A_1}; V^n) \tag{4.38}$$

and

$$I(\overline{A_1'A_2'}; V^n) = D(\overline{B_0B_2}; V^n) \tag{4.39}$$

§3. $\vec{q}(A_2')$ is detemined in terms of $\vec{q}(B_0)$, $\vec{q}(B_1)$, $\vec{q}(B_2)$, and $\vec{q}(B_1')$ by assuming equation (4.23) and

$$I(\overline{A_2'A_1'}; V^n) = D(\overline{B_0B_2}; V^n) \tag{4.40}$$

Note that, in §5, $\vec{q}(B_1')$ is determined in terms of $\vec{q}(B_2)$, $\vec{q}(B_3)$, and $\vec{q}(B_4)$.

§4. $\vec{q}(B_0')$ is determined in terms of $\vec{q}(A_1')$, $\vec{q}(B_2)$ and $\vec{q}(B_3)$ by assuming equation (4.25) and

$$I(\overline{B_0'B_1'}; V^n) = D(\overline{B_2B_3}; V^n) \tag{4.41}$$

§5. $\vec{q}(B_1')$ is determined in terms of $\vec{q}(B_2)$, $\vec{q}(B_3)$, and $\vec{q}(B_4)$ by assuming

$$I(\overline{B_1'B_0'}; V^n) = D(\overline{B_2B_3}; V^n) \tag{4.42}$$

and

$$I(\overline{B_1'B_2'}; V^n) = D(\overline{B_3B_4}; V^n) \tag{4.43}$$

§6. $\vec{q}(B_2')$ is determined in terms of $\vec{q}(B_3)$, $\vec{q}(B_4)$, $\vec{q}(C_0)$ and $\vec{q}(C_1)$ by assuming

$$I(\overline{B_2'B_1'}; V^n) = D(\overline{B_3B_4}; V^n) \tag{4.44}$$

and

$$I(\overline{B_2'B_3'}; V^n) = D(\overline{C_0C_{1/2}}; C_0, C_1; V^n) \tag{4.45}$$

§7. $\vec{q}(B_3')$ is determined in terms of $\vec{q}(C_0)$ and $\vec{q}(C_1)$ by assuming

$$I(\overline{B_3'B_2'}; V^n) = D(\overline{C_0C_{1/2}}; C_0, C_1; V^n) \tag{4.46}$$

and

$$I(\overline{B_3'B_4'}; V^n) = D(\overline{C_{1/2}C_1}; C_0, C_1; V^n) \tag{4.47}$$

§8. $\vec{q}(B_4')$ is determined in terms of $\vec{q}(C_0)$, $\vec{q}(C_1)$ and $\vec{q}(C_1')$ by assuming equation (4.33) and

$$I(\overline{B_4'B_3'}; V^n) = D(\overline{C_{1/2}C_1}; C_0, C_1; V^n) \tag{4.48}$$

Note that, in §10, $\vec{q}(C_1')$ is determined in terms of $\vec{q}(C_1)$ and $\vec{q}(C_2)$.

§9. $\vec{q}(C_0')$ is determined in terms of $\vec{q}(C_1)$, $\vec{q}(C_2)$, and $\vec{q}(B_3')$ by assuming equation (4.35) and

$$I(\overline{C_0'C_1'}; V^n) = D(\overline{C_1C_2}; V^n) \tag{4.49}$$

§10. $\vec{q}(C_1')$ is determined in terms of $\vec{q}(C_1)$ and $\vec{q}(C_2)$ by assuming

$$u(C_1') = u(C_2) \tag{4.50}$$

and

$$I(\overline{C_1'C_0'}; V^n) = D(\overline{C_1C_2}; V^n) \tag{4.51}$$

Note that:

(a) Equations (4.37)–(4.49) and (4.51) imply that the reconstructed $\{\vec{q}\}$ does indeed satisfy the D-flux conservation condition if it is specified using the second SGVR procedure described above.

(b) We have

$$I(\overline{P'Q'}; V^n) = I(\overline{Q'P'}; V^n) = D(\overline{PQ}; V^n) \tag{4.52}$$

if (i) P and Q are two neighboring original grid points, (ii) P' and Q' are two neighboring reconstructed grid points, (iii)

$$x(P) = x(P') < x(Q') = x(Q) \tag{4.53}$$

and (iv) $\vec{q}(P')$ and $\vec{q}(Q')$ are specified using the second SGVR procedure. On the other hand, generally

$$I(\overline{P'Q'}; V^n) \neq I(\overline{Q'P'}; V^n) \tag{4.54}$$

if $\vec{q}(P')$ and $\vec{q}(Q')$ are specified using the first SGVR procedure. In this sense the second procedure is less "discriminating" than the first procedure. Generally, the numerical results obtained using the second procedure is also slightly less accurate than those obtained using the first procedure. However, the second procedure is more robust and, as will be shown, easier to be extended for multidimensional applications.

(c) Based on numerical evidence, it appears that incorporation of the current SGVR procedure into the 1D basic LTS procedure described in Section 3 does not have a negative impact on the stability of the latter procedure. It is expected that the same conclusion is also valid in 2D and 3D cases (the 2D and 3D SGVR procedures are the topics to be discussed below).

Based on the background information provided in Section 3 regarding the 2D and 3D CESE solvers, multidimensional extensions of the above second SGVR procedure are discussed in the following remarks:

(a) Consider a case where two triangle-based 2D spatial grids (referred to as the "original" and "reconstructed" grids, respectively) be given at $t = t^n$. Let the original (reconstructed) grid be divided into different spatial LTS grid zones which are the top (bottom) faces of various space-time LTS grid zones. As explained in Section 3, for either of these grids, the spatial domain at $t = t^n$ is filled by the quadrilaterals which are the spatial projections of the BCEs. In addition, a triple of neighboring quadrilaterals always meets at a common vertex and fills the spatial domain surrounding this vertex. Moreover, the number of the independent solution points that share the same spatial location and are associated with the common vertex is equal to the number of different spatial LTS grid zones converge at this vertex. In the following, it will be explained how the reconstructed grid values can be determined in terms of the known original grid values without violating

the D-flux conservation condition over the time level $t = t^n$.

(b) Let (j, k, n) denote a solution point lying in the interior of a reconstructed spatial LTS grid zone. Then the unknowns U^n_{jk}, $(u_x)^n_{jk}$, and $(u_y)^n_{jk}$ can be determined in terms of the original grid values by assuming that, over each of the three quadrilaterals associated with (j, k, n), the I-flux evaluated using the three unknowns is equal to the D-flux evaluated using the original grid values (how this D-flux is evaluated will be explained later). These conditions are essentially extensions of the conditions such as equations (4.38) and (4.39). Note that: (i) for a reconstructed solution point where two or more different LTS grid zones meet, the grid values may be determined using a combination of finite-difference and D-flux conservation conditions—essentially extensions of the conditions such as equations (4.23) and (4.40); and (ii) as will be shown immediately, the D-flux over a reconstructed quadrilateral is evaluated in terms of the original grid values using a rule that is essentially an extension of equation (4.6).

(c) Each quadrilateral referred earlier is the common subset of the SEs of two neighboring solution points (Wang and Chang 1999a, Zhang *et al.* 2002). Let these two solution points be referred to as the cohosts of the quadrilateral. Then the D-flux over any subset of an original quadrilateral is defined to be the simple average of the I-fluxes evaluated using the grid values of the co-hosts of the quadrilateral. Moreover, the D-flux over a given reconstructed quadrilateral is defined to be the sum of a set of component D-fluxes—each component represents the D-flux over the nonnull intersection of the reconstructed quadrilateral and one of the original quadrilaterals, and is evaluated in terms of the grid values of the co-hosts of the original quadrilateral that contains the intersection.

(d) Consider a case where quadrilateral-based original and reconstructed 2D spatial grids are given at $t = t^n$. Let (j, k, n) denote a solution point lying in the interior of a reconstructed spatial LTS grid zone. Then, for (j, k, n), the number of the associated quadrilaterals (which is four) is greater than that of associated unknowns (which is three). Because the three unknowns generally become over-determined if a flux condition is imposed over each of the four quadrilaterals, the recipe described above in item (a) obviously cannot be used here to evaluate the three unknowns. However, as will be shown, these unknowns can be determined using an alternative based on the least square method.

(e) Let (i) the values of the three unknowns be denoted by v_1, v_2, and v_3, respectively; (ii) the four quadrilaterals be denoted by $Q(1), Q(2), Q(3)$, and $Q(4)$, respectively; (iii) the I-flux over $Q(j)$ evaluated using v_1, v_2, and v_3 be denoted by f_j; and (iv) the D-flux over $Q(j)$ evaluated using the known original grid values be denoted by d_j. Then (Zhang *et al.* 2002)

$$f_j = \sum_{k=1}^{3} g_{jk} v_k, \quad j = 1, 2, 3, 4 \tag{4.55}$$

where g_{jk} are known geometry-related coefficients. Let $v_k (k = 1, 2, 3)$ be such that

$$S(v_1, v_2, v_3) \equiv \sum_{j=1}^{4} (f_j - d_j)^2 \tag{4.56}$$

is at its minimum, i.e.

$$\frac{\partial S}{\partial v_i} = 0, \quad i = 1, 2, 3 \tag{4.57}$$

Then, with the aid of equation (4.55), one concludes that

$$\sum_{k=1}^{3} h_{ik} v_k = b_i \tag{4.58}$$

where

$$h_{ik} \equiv \sum_{j=1}^{4} g_{ji} g_{jk} \text{ and } b_i \equiv \sum_{j=1}^{4} d_j g_{ji}, \quad i, k = 1, 2, 3 \tag{4.59}$$

Thus $v_k (k = 1, 2, 3)$ can be determined using equation (4.58) if the square matrix formed by $h_{ik} (i, k = 1, 2, 3)$ is nonsingular. As a result of its definition, the aforementioned matrix is symetric and nonsingular if the three columns of of the 4×3 matrices formed by $g_{jk} (j = 1, 2, 3, 4)$ and $k = 1, 2, 3)$ are linearly independent (Strang 1988).

(f) For a standard 3D CESE solver with a tetrahedron-based spatial grid, (i) the number of BCEs and the number of the unknowns associated with an interior solution point are identical (both are four), and (ii) the spatial projection of each BCE is a hexahedron with five vertices. Thus, for this case, a 3D reconstruction procedure can be built using a set of recipes similar to those described in item (a).

(g) On the other hand, for a 3D CESE solver with a hexahedron-based spatial grid, (i) there are six BCEs and four unknowns associated with an interior solution point, and (ii) the spatial projection of each BCE is an octahedron with six vertices. Thus, for this case, a 3D reconstruction procedure can be built using a set of recipes similar to those given in item (b).

5. Numerical experiments

A series of numerical experiments has been conducted to examine the capability and robustness of the LTS and SGVR procedures described in Sections 3 and 4, respectively. Note that: (i) in the first numerical example involving

equation (2.1), the left boundary values are specified using the given left boundary data while the right boundary values are evaluated using equation (3.23); (ii) in other numerical examples involving systems of 1D conservation laws, the boundary values of each conservative variable are specified using the non-reflecting boundary conditions in the form of equation (3.24); (iii) the first SGVR procedure described in Section 4 or its extensions for systems of 1D conservation laws is used in each of numerical examples to be considered; and (iv) without exception, the numerical solutions to be presented are obtained assuming that $\alpha = 1$ in the a-α scheme or its extensions.

The first example involves a numerical solution to equation (2.1) with $a = 1$. The exact solution is assumed to be

$$u = \frac{10}{\sqrt{\pi}} \exp\left[-100(x - t - 0.3)^2\right] \tag{5.1}$$

It represents a Guassian pulse moving in the x direction with the constant speed of unit. As such, (i) the initial and left boundary values needed for numerical solution are evaluated using equation (5.1); and (ii) the Guassian peak is located at $x = t + 0.3$ at any time t, i.e. it is located at $x = 0.3$ when $t = 0$.

To obtain the numerical solution, a uniform space-time coarse grid with $\Delta x = 0.01$ and $\Delta t = 0.009$ (i.e. the CFL number $= 0.9$) is first applied to cover the whole computational domain. A uniform fine-grid zone with $R = 10$ and a fixed spatial length of 0.22 is then introduced to enhance the resolution near the peak. The left boundary of the fine-grid zone is placed at $x = 0.2$ when $t = 0$. It moves in the positive x direction every two or three coarse time intervals so that the Guassian peak and the mean spatial location of the fine-grid zone are kept within a spatial distance of 0.01. The exact and numerical solutions (denoted by a solid line and dots, respectively) along with the spatial grid distribution at $t = 0.9$ are depicted in figure 8. Not only the numerical solution agrees very well with the exact solution throughout the entire domain, the numerical data also matches smoothly across the two interfaces separating the fine- and coarse-grid zones.

Also noted are: (i) according to equation (5.1), at $t = 0.9$, $u \doteq 5.6418$ at $x = 1.1995$ and $x = 1.2005$ (i.e. the two fine grid locations closest to the location $x = 1.2$ where the peak value of the Guassian pulse occurs); and (ii) on the other hand, according to the numerical solution, $u \doteq 5.6416$ at the same two locations. The numerical error is less than 0.004%.

In the second example, the Sod shock tube problem (Chang 1995) is solved using the Euler version of the dual a-α scheme along with the present LTS-SGVR procedure. The specific-heat ratio γ is 1.4 and the spatial domain is $[-0.5, 0.5]$. The initial conditions are: $(\rho, v, p) = (1, 0, 1)$ if $x < 0$ and $(\rho, v, p) = (0.125, 0, 0.1)$ if $x > 0$, where ρ, v and p denote the normalized density, velocity and pressure, respectively. The underlying coarse grid with $\Delta x = 4 \times 10^{-3}$ covers the entire spatial domain, while the fine-grid zone of a fixed spatial length covers the region $[-0.05, 0.05]$ at $t = 0$ and moves with the shock thereafter. The time-step size Δt is 1.5×10^{-3} (i.e. the CFL number ≈ 0.82) and the grid refinement ratio $R = 4$. The overall flow distributions at $t = 0.195$ are shown in figure 9a. A close-up view covering the neighborhood of the fine-grid zone is presented in figure 9b (the dots represent grid solutions). The shock is well resolved. No numerical oscillation is observed even though the fine-grid zone moves with the shock after $t = 0$. Extensive calculations have also been carried out for a wide range of the values of R. Results all indicate sharp, smooth transient at grid interfaces, even for a high refinement ratio of $R = 64$.

The third example deals with detonation propagation in a one-dimensional tube using an extended dual a-α scheme (Wu *et al.* 2004). The chemical kinetics scheme involves a one-step, irreversible, Arrhenius-type reaction for two species (i.e. reactant and product),

$$\text{Reactant}(R) = \text{Product}(P) + \text{heat release}(q) \tag{5.2}$$

The mass production rate of the reactant per unit volume is

$$\dot{\omega}_R = -\rho Y_R A_f \exp(-T_f/T) \tag{5.3}$$

where A_f and T_f are the pre-exponential factor and the activation temperature, respectively. Their values and other parameters adopted in the calculations are $\gamma = 1.25$, $MW = 15\,\text{kg/kmol}$, $q = 6.79 \times 10^6\,\text{J/kg}$, $A_f = 7.5 \times 10^9\,1/\text{s}$, $T_f = 15000\,\text{K}$, where MW stands for the molecular weight.

Figure 10 shows the computational domain and initial conditions. The tube spans a length of 20 cm with a closed head end and an open exit. Initially, the reactant at 1 atm and 300 K fills up the tube. A small energetic region with $p = 30\,\text{atm}$ and $T = 3000\,\text{K}$ is placed at the head end to initiate detonation. Two uniform spatial grids are used in the calculations. One is the underlying coarse grid that covers the entire computational domain, and the other is a fine grid that has a fixed length of 3 cm and travels with the

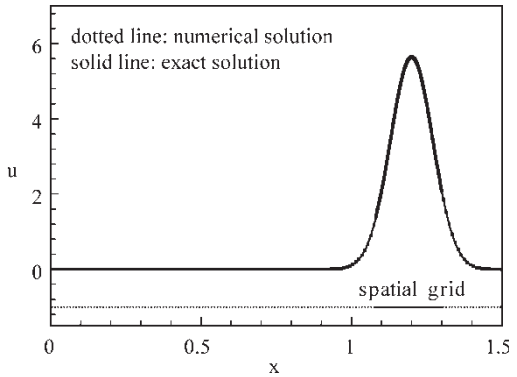

Figure 8. Exact and numerical solutions along with grid distribution at $t = 0.9$ for the case of scalar wave propagation ($R = 10$).

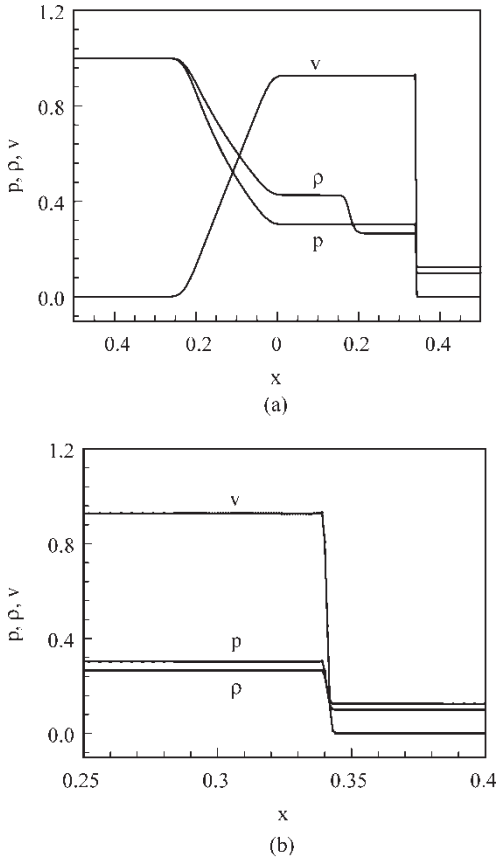

Figure 9. Numerical solution to Sod's shock problem at $t = 0.195$ ($R = 4$), (a) distributions of pressure, density, and velocity in entire domain, (b) close-up view near the shock.

detonation wave to enhance the resolution of the wave front. The number of the grid points of the coarse grid is fixed to 2001 (i.e. $\Delta x = 0.01$ cm) for all the simulations. The number of the grid points of the fine grid is determined by the refinement ratio R.

A series of simulations has been carried out with $R = 1, 2, 4,$ and 8. Different from the previous two examples in which the temporal intervals on the coarse grids are fixed, the CFL numbers based on the coarse grid size are taken to be 0.9, 0.6, 0.6 and 0.45 for these grid refinement ratios, respectively. Table 1 summerizes the numerical predictions of the characteristic properties of the flow with various R's. Also included in the table are their theoretical counterparts calculated based on the the Zeldovich, von Neumann and Döring (ZND) theory (Wu 2002, Wu *et al.* 2004). The calculated von

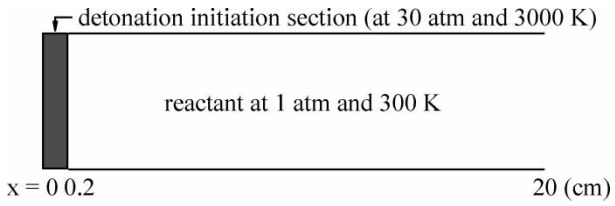

Figure 10. Initial conditions used in the case of detonation propagation.

Table 1. Comparison of numerical results for different mesh refinement ratio R's with theoretical counterparts for the case of detonation propagation.

R	u_D m/s	p_s atm	p_{CJ} atm	T_{CJ} K	p_h atm
1	2849	27.0	22.1	3743	8.06
2	2850	29.0	22.1	3743	8.06
4	2850	32.2	22.1	3743	8.06
8	2850	36.0	22.1	3743	8.06
Theoretical value	2837	42.9	22.0	3736	8.05

Neumann spike pressure, p_s, approaches the theoretical value with increasing R. The detonation wave velocity u_D, the pressure p_{CJ} and temperature T_{CJ} at the Chapman–Jouguet state, and the pressure at the head end p_h are well predicted with all R's. It is worth mentioning that the deviation of the calculated p_s from the theoretical prediction results from the assumptions employed in the ZND theory that an inert shock exists in the detonation wave front, and that the flow properties are uniformly distributed immediately downstream of the shock. These assumptions apparently do not reflect the actual flow evolution predicted by the numerical calculation, in which flow continuously expands downstream of the shock and chemical reactions start to occur during this process. The calculated p_s based on a finite-rate chemcial kinetics model tends to be lower than that predicted by the ZND theory.

All the numerical schemes, including the space-time CE/SE method, must introduce more or less artificial dissipation to suppress numerical oscillations near steep gradients in flowfields. For the present detonation problem, the a-α scheme has been used with $\alpha = 1$ in all the calculations. As a consequence, numerical dissipation is introduced near the detonation wave front, leading to a smeared wave front. Since numerical dissipation decreases with increasing grid resolution, the numerically predicted von Neumann pressure spike increases with R. In comparison, the detonation wave speed u_D and the CJ state are only functions of the total heat release with fixed gas properties, and the pressure at the chamber head end p_h depends only on p_{CJ}.

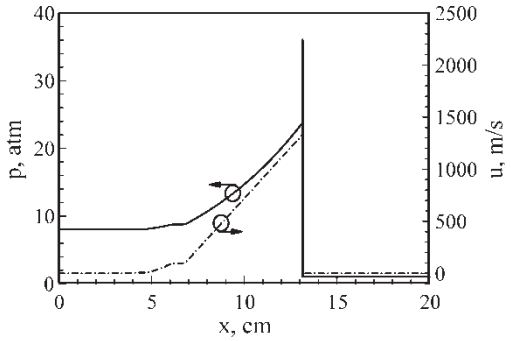

Figure 11. Snapshot of pressure and velocity distributions at 45 μs for the case of detonation propagation ($R = 8$).

These values are not affected by the von Neumann pressure spike and, therefore, can be accurately predicted even with a simple coarse mesh.

To further examine the performance of the LTS procedure developed in the present work, the snapshot of the pressure and velocity fields at $t = 45.4\,\mu s$ for the case of $R = 8$ is plotted in figure 11. The left coarse/fine grid interface is located at 10.33 cm at this instant time. No numerical oscillations exist at any place in the domain even after the fine grid has moved over a long distance from its initial position at the chamber head-end. The LTS procedure developed herein is indeed capable of providing accurate solutions across coarse/fine grid interfaces.

6. Conclusions

A new local time-stepping procedure within the framework of the space-time CESE method has been established. The scheme is compatible with unstructured spatial grids and capable of treating one- and multi-dimenisonal problems. With the aid of spatial grid value reconstruction, the present time stepping procedure is applicable to situations requiring that fine grid zones be moved with time. Moreover, by taking advantage of several key features of the CESE method, flux conservation across an interface separating grid zones of different time-step sizes is enforced in a much simpler and more efficient manner compared with existing approaches. Thus, even without using any correction pass, no spurious reflections originated from such an interface are observed in the numerical experiments presented herein. For a variety of flow problems involving moving shock and flame discontinuities, accurate and robust numerical simulations can be carried out even with a reduction in time-step size on the order of 10 or higher.

Acknowledgements

This work was supported partly by the NASA Glenn Research Center and partly by the DoD Multidisciplinary University Research Initiative under ONR Grant No. N00014-99-1-0744. Yuhui Wu and Vigor Yang wish to thank Dr Gabriel Roy for his support and encouragement.

References

Bell, J., Berger, M.J., Saltzman, J. and Welcome, M., Three-dimensional adaptive mesh refinement for hyperbolic conservation laws. *SIAM J. Sci. Comput.*, 1994, **15**, 127–138.

Berger, M.J., On conservation at grid interfaces. *SIAM J. Numer. Anal.*, 1987, **24**, 967–984.

Berger, M.J. and Colella, P., Local adaptive mesh refinement for shock hydrodynamics. *J. Comput. Phys.*, 1989, **82**, 64–84.

Berger, M.J. and LeVeque, R.J., Adaptive mesh refinement using wave-propagation algorithms for hyperbolic systems. *SIAM J. Numer. Anal.*, 1998, **35**, 2298–2316.

Berger, M.J. and Oliger, J., Adaptive mesh refinement for hyperbolic partial differential equations. *J. Comput. Phys.*, 1984, **53**, 484–512.

Chang, S.C., The method of space-time conservation element and solution element—a new approach for solving the Navier–Stokes and Euler equations. *J. Comput. Phys.*, 1995, **119**, 295–324.

Chang, S.C., Courant Number Insensitive CE/SE Schemes, AIAA Paper-2002-3890, 2002.

Chang, S.C. and Wang, X.Y., Multidimensional Courant Number Insensitive CE/SE Euler Solver for Applications Involving Highly Nonuniform Meshes, AIAA Paper-2003-5280, 2003.

Chang, S.C., Yu, S.T., Himansu, A., Wang, X.Y., Chow, C.Y. and Loh, C.Y., The method of space-time conservation element and solution element—a new paradigm for numerical solution of conservation laws. In Computational Fluid Dynamics Review 1998, edited by M.M. Hafez and K. Oshima, Vol. 1, 1998 (World Scientific: Singapore).

Chang, S.C., Wang, X.Y. and Chow, C.Y., The space-time conservation element and solution element method: A new high-resolution and genuinely multidimensional paradigm for solving conservation laws. *J. Comput. Phys.*, 1999, **156**, 89–136.

Chang, S.C., Wang, X.Y. and To, W.M., Application of the space-time conservation element and solution element method to one-dimensional convection–diffusion problems. *J. Comput. Phys.*, 2000, **165**, 189–215.

Chang, S.C., Himansu, A., Loh, C.Y., Wang, X.Y. and Yu, S.T., Robust and Simple Non-Reflecting Boundary Conditions for the Euler Equations—A New Approach Based on the Space–Time CE/SE Method, NASA TM-2003-212495 2003.

Strang, Gilbert, *Linear Algebra and its Applications*, 3rd ed., 1988 (Saunders).

Wang, X.Y. and Chang, S.C., A 2D non-splitting unstructured triangular mesh Euler solver based on the space-time conservation element and solution element methods. *Comput. Fluid Dynam J.*, 1999a, **8**, 309–325 (Note: In this paper, the factor (Δt/4) should be inserted in front of the last term in each of Eqs. (53), (54), (56), and (57)).

Wang, X.Y. and Chang, S.C., A 3D Structured/Unstructured Euler Solver Based on the Space-Time Conservation Element and Solution Element Method, AIAA Technical Paper 3278, 1999b.

Wu, Y.H., System Performance and Thermodynamic Cycle Analysis of Air-Breathing Pulse Detonation Engines, Ph.D. Dissertation, 2002, Department of Mechanical and Nuclear Engineering, Pennsylvania State University, University Park, Pennsylvania.

Wu, Y.H., Ma, F.H. and Yang, V., System performance and thermodynamic cycle analysis of airbreathing pulse detonation engines. *J. Propul. Power*, 2003, **19**, 556–567.

Wu, Y.H., Ma, F.H. and Yang, V., Space-time method for detonation problems with finite rate chemical kinetics. *Int. J. Comput. Fluid Dynam.*, 2004, **18**, 277–287.

Zhang, Z.C., Yu, S.T. and Chang, S.C., A space-time conservation element and solution element method for solving the two- and three-dimensional unsteady Euler equations using quadrilateral and hexahedral meshes. *J. Comput. Phys.*, 2002, **175**, 168–199.